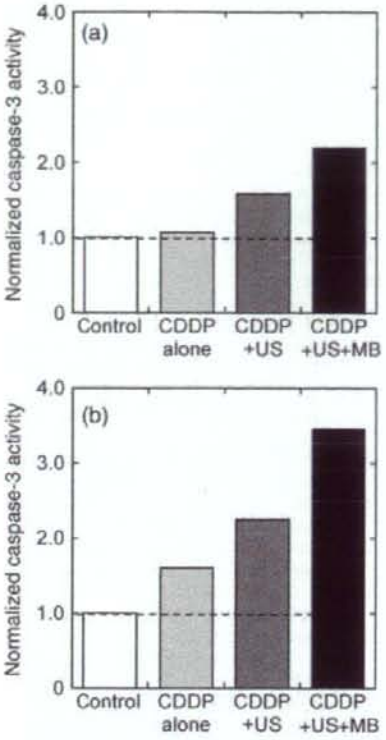

Fig. 4. Upregulation of the proapoptotic gene caspase-3. Colon 26 cells were treated with cis-diamminedichloroplatinum (II) (CDDP) (10 μmol/L) in the presence of ultrasound (US) with and without microbubbles (MB). Caspase-3 activity was measured at 24 h after treatment. Twelve wells from 48-well plates were analyzed for each condition. Results are expressed as the number of molecules of p-nitroaniline (pNA) (nmol) released by 1 mg of protein in (a) 1 and (b) 2 h. Ultrasound intensity 1.0 W/cm^2; duty cycle 50%; number of pulses 2000; pulse repletion frequency 250 Hz; and exposure time 10 s.

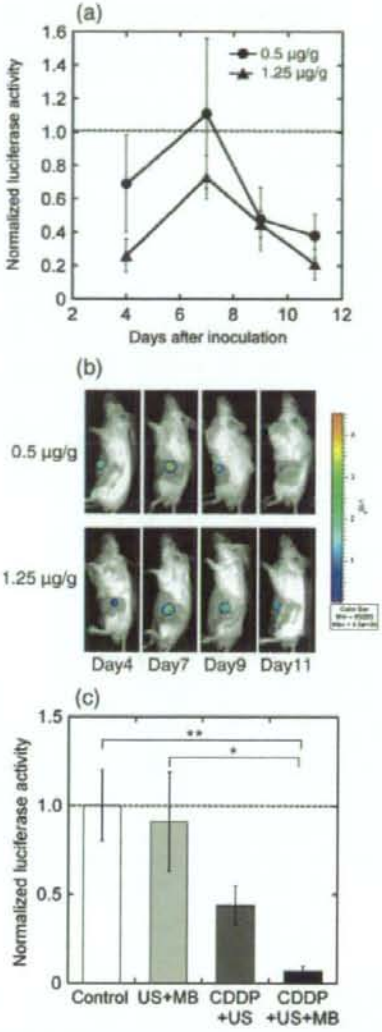

Fig. 5. Antitumor effects of cis-diamminedichloroplatinum (II) (CDDP) + ultrasound (US) + microbubbles (MB) on HT29-luc xenografts with two different CDDP concentrations (0.5 and 1.25 μg/g bodyweight) on days 4, 7, 9, and 11. Ultrasound intensity 3.0 W/cm^2; duty cycle 20%; number of pulses 200; pulse repletion frequency 1000 Hz; and exposure time 60 s. Luciferase activity after (a) treatment and (b) bioluminescence imaging. The luciferase activity under each concentration of CDDP + US + MB was normalized with each concentration of CDDP + US. CDDP (0.5 μg/g bodyweight) + US ($n = 4$), CDDP (0.5 μg/g bodyweight) + US + MB ($n = 4$), CDDP (1.25 μg/g bodyweight) + US ($n = 4$), CDDP (1.25 μg/g bodyweight) + US + MB ($n = 4$). (c) The luciferase activity normalized with that of control at day 11, where the concentration of CDDP was 1.25 μg/g bodyweight. Control ($n = 5$), US + MB ($n = 4$). The bars represent mean ± SEM. $^*P < 0.05$, $^{**}P < 0.01$.

groups. These effects were recognized by bioluminescence images (Fig. 5b). Figure 5c shows antitumor effects for different conditions (US + MB, CDDP + US, CDDP + US + MB) at day 11, where the CDDP concentration was 1.25 μg/g bodyweight, and the bioluminescence of each condition was normalized with that of the control at day 11. There was no significant difference between control and US + MB. CDDP alone was recognized as the difference between US + MB and CDDP + US, where CDDP alone decreased US + MB by 48.4%. MB further reduced CDDP + US by 84.1%.

Discussion

The US–MB method permeabilizes the cell membrane directly, thereby allowing the delivery of exogenous molecules into the cells. Electroporation is also a method that is used to permeabilize the cell membrane by direct application of an external electric field. Cemazar *et al.* delivered CDDP into both murine sarcoma cisplatin-sensitive TBL.C12 cells and their resistant subclones, namely, TBL.C12.Pt cells.[27] These cells were treated *in vivo* by electroporation, and their platinum content was measured by atomic absorption. Based on their findings, the authors suggested that 10^6 platinum molecules were delivered into TBL.C12 and TBL.C12.Pt cells at 0.05 and 0.46 μg/mL, respectively, where these concentrations correspond to the 50% inhibitory concentration values of platinum for these cells. Our finding that 10^6–10^7 calcein molecules were internalized per cell at 200 μmol/L, as shown in Figure 1a, is in agreement with the finding of Cemazar *et al.* and demonstrates that US–MB permeabilization is as efficient as electroporation in the permeabilization of cell membranes.

There are several anticancer drugs with a similar molecular weight to CDDP. For example, the molecular weight of vincristine is 923, and that of taxol is 854. There is not even one order difference between these molecules and cisplatin, which has a molecular weight of 300. Therefore, we think that the same number of molecules will be delivered into cells by this method. However, it is noted that the number of molecules internalized is not directly correlated with subsequent antitumor effects.

Following the application of MB and US, the cell membrane surface becomes rough and is characterized by depressions that are reversible within 24 h after US exposure.[28,29] Collapsed MB or cavitation bubbles generated by collapsed MB induce impulsive pressures such as liquid jets and shock waves; these pressures affect the neighboring cells. The shock wave propagation distance from the center of a cavitation bubble that has the potential to damage the cell membrane is considerably larger than the maximum radius of the cavitation bubble.[8] Molecular dynamic simulation has revealed that the cell membrane affected by the shock wave is deformed, thereby allowing the entry of exogenous molecules into the cells.[30] Although the membrane permeabilization time has not been measured accurately, it has been reported that the membrane reseals within 80 s when it is permeabilized by shock waves.[31] When 1176 water molecules are delivered into a lipid bilayer comprising 128 dipalmitoylphosphatidylcholine molecules, a water pore of 1.9-nm diameter is formed in the lipid bilayer;[30] this water pore is larger than the CDDP with a diameter of 0.48 nm.

As shown in Figure 1, the US–MB method enhances cell permeability, thereby allowing the delivery of a large number of CDDP molecules into the cells. The combination of high-intensity ultrasound (shock waves) and generated cavitation bubbles – the same concept as that used in the US–MB method – can deliver CDDP molecules into the cells.[32–35] However, the cytotoxicity of CDDP depends on the cell type (Fig. 2); therefore, resistance to CDDP is not completely overcome simply by the application of US and MB (or cavitation bubbles).

The delivery of CDDP into cells induces apoptosis.[36] Apoptotic pathways involved in mediating CDDP-induced cellular effects have been investigated thoroughly.[37] The apoptotic induction resulting from CDDP delivery was confirmed by DAPI staining (Fig. 3) and measurement of caspase-3 activity (Fig. 4). The upregulation of caspase-3 coincides with the observations of previous reports.[10,11,38,39] Caspase-3 is a key effector of apoptosis that is responsible for the proteolytic cleavage of cytoskeletal proteins, kinase, and DNA repair enzymes.[40] The signaling pathway that mediates US-induced apoptosis has been investigated previously.[11,41]

In the *in vivo* experiments, CDDP and MB were injected intratumorally on days 3, 7, and 10 after the injection with tumor cells (HT29-luc), and the tumor was exposed to US. The normalized luciferase activity increased by day 7 and decreased afterwards. This indicates that the antitumor effects resulted from the activity of MB becoming dominant against the tumorigenesity. Tumor growth was suppressed effectively, indicating that the US–MB method provides a synergistic effect with antitumor drugs.[42,43]

We used a local administration system in the *in vivo* experiments (direct injection of CDDP + MB and local US exposure). This local exposure to US has more advantages than the currently available local therapies such as surgery and radiotherapy. However, the usefulness of local therapy is expected to be limited to a particular tumor or a particular tumor stage. For example, hepatocellular carcinomas and brain gliomas seldom metastasize to other organs. Instead, hepatocellular carcinomas and gliomas grow within the liver and brain, respectively, and eventually cause death without metastasizing to other organs. Because these tumors are fed by a tumor-feeding artery, the arterial injection of any anticancer agent (ACA) into the tumor-feeding artery is the most direct way of delivering it into the tumors, mainly because of the first-path effect. With regard to superficial bladder cancer recurrences, half of all such cases recur, and 10–30% progress to a higher grade or stage and form local invasive cancer. Intravesical administration of ACA is known to prolong the duration of progression-free survival. For a clinically randomized phase III trial conducted in patients with stage III ovarian cancer, local intraperitoneal injection of ACA can prolong the duration of overall survival, compared to systemic intravenous injection.[44]

According to the above mentioned evidence, we believe that it is possible to establish a local ACA delivery system in experimental animal models in anticipation of future clinical trials. The US–MB method has the advantages of tissue specificity and non-invasiveness. In addition, this method can be applied repeatedly to patients without immunogenicity.[21] However, the efficiency of molecular delivery into cells is low, and the subsequent bioeffects are not adequate to be investigated by clinical trials. Recently, many types of MB with characteristics of tissue specificity and drug incorporation have been developed[45] and the US exposure conditions have been investigated.[46,47] Combination of the US–MB method with other physical methods such as hyperthermia has also been investigated.[48] In our laboratory, we have investigated the relationship between the physicochemical properties (zeta potential, size, and lipid components) of MB and the transfection efficiency (data not shown).

In conclusion, in the present study we have demonstrated that the US–MB method combined with the well-known chemotherapeutic agent CDDP has great therapeutic potential in cancer therapy. By reducing the dose of CDDP required to induce cell death through the abovementioned method it may be possible to increase the therapeutic action of the drug and to limit the toxicity of the treatment.

Acknowledgments

We thank Fuki Oosawa for her technical assistance. S.M. acknowledges Grant-in-Aid for Scientific Research (B) (19390507) and H.M. acknowledges Grant-in-Aid for Scientific Research (B) (19592334). G.V. acknowledges the program and projects grants from Cancer Research, UK, Institut national de la santé et de la recherche médicale (INSERM), Ligue Contre le Cancer and support through grant 0607-3D1615–66/AO INSERM from the French National Cancer Institute. T.K. acknowledges Grant-in-Aid for Scientific Research (B) (20300173), and Grant-in-Aid for Scientific Research on Priority Area MEXT (20015005). Y.M. and T.K. acknowledge Grant for Research on Nanotechnical Medical, the Ministry of Health, Labour, and Welfare of Japan (H19-nano-010). G.V. and T.K. acknowledge the Japan–France Integrated Action Program Joint Project. CDDP was donated by Nihon Kayaku (Tokyo, Japan).

References

1 Klibanov AL. Ligand-carrying gas-filled microbubbles: ultrasound contrast agents for targeted molecular imaging. *Bioconjug Chem* 2005; **16**: 9–17.

2 Harvey CJ, Blomley MJ, Eckersley RJ, Cosgrove DO. Developments in ultrasound contrast media. *Eur Radiol* 2001; **11**: 675–89.

3 Barak M, Katz Y. Microbubbles: pathophysiology and clinical implications. *Chest* 2005; **128**: 2918–32.

4 Lindner JR. Molecular imaging with contrast ultrasound and targeted microbubbles. *J Nucl Cardiol* 2004; **11**: 215–21.

5 Chen WS, Matula TJ, Crum LA. The disappearance of ultrasound contrast bubbles: observations of bubble dissolution and cavitation nucleation. *Ultrasound Med Biol* 2002; **28**: 793–803.

doi: 10.1111/j.1349-7006.2008.00989.x

6 Miller DL, Dou C. Membrane damage thresholds for 1- to 10-MHz pulsed ultrasound exposure of phagocytic cells loaded with contrast agent gas bodies *in vitro*. *Ultrasound Med Biol* 2004; **30**: 973–7.
7 Hallow DM, Mahajan AD, McCutchen TE, Prausnitz MR. Measurement and correlation of acoustic cavitation with cellular bioeffects. *Ultrasound Med Biol* 2006; **32**: 1111–22.
8 Kodama T, Tomita Y, Koshiyama K, Blomley MJ. Transfection effect of microbubbles on cells in superposed ultrasound waves and behavior of cavitation bubble. *Ultrasound Med Biol* 2006; **32**: 905–14.
9 Feril LB Jr, Tsuda Y, Kondo T *et al*. Ultrasound-induced killing of monocytic U937 cells enhanced by 2,2'-azobis (2-amidinopropane) dihydrochloride. *Cancer Sci* 2004; **95**: 181–5.
10 Firestein F, Rozenszajn LA, Shemesh-Darvish L, Elimelech R, Radnay J, Rosenschein U. Induction of apoptosis by ultrasound application in human malignant lymphoid cells: role of mitochondria–caspase pathway activation. *Ann NY Acad Sci* 2003; **1010**: 163–6.
11 Honda H, Kondo T, Zhao QL, Feril LB Jr, Kitagawa H. Role of intracellular calcium ions and reactive oxygen species in apoptosis induced by ultrasound. *Ultrasound Med Biol* 2004; **30**: 683–92.
12 Chaussy C, Thuroff S, Rebillard X, Gelet A. Technology insight: high-intensity focused ultrasound for urologic cancers. *Nat Clin Pract Urol* 2005; **2**: 191–8.
13 Colombel M, Gelet A. Principles and results of high-intensity focused ultrasound for localized prostate cancer. *Prostate Cancer Prostatic Dis* 2004; **7**: 289–94.
14 Hou CC, Wang W, Huang XR *et al*. Ultrasound–microbubble-mediated gene transfer of inducible Smad7 blocks transforming growth factor-β signaling and fibrosis in rat remnant kidney. *Am J Pathol* 2005; **166**: 761–71.
15 Shimamura M, Sato N, Taniyama Y *et al*. Gene transfer into adult rat spinal cord using naked plasmid DNA and ultrasound microbubbles. *J Gene Med* 2005; **7**: 1468–74.
16 Takahashi M, Kido K, Aoi A, Furukawa H, Ono M, Kodama T. Spinal gene transfer using ultrasound and microbubbles. *J Control Release* 2007; **117**: 267–72.
17 Gambihler S, Delius M, Ellwart JW. Permeabilization of the plasma membrane of L1210 mouse leukemia cells using lithotripter shock waves. *J Membr Biol* 1994; **141**: 267–75.
18 Kodama T, Doukas AG, Hamblin MR. Shock wave-mediated molecular delivery into cells. *Biochim Biophys Acta* 2002; **1542**: 186–94.
19 Boulikas T, Vougiouka M. Cisplatin and platinum drugs at the molecular level. *Oncol Reports* 2003; **10**: 1663–82.
20 Tennant JR. Evaluation of the trypan blue technique for determination of cell viability. *Transplantation* 1964; **2**: 685–94.
21 Aoi A, Watanabe Y, Mori S, Takahashi M, Vassaux G, Kodama T. Herpes simplex virus thymidine kinase-mediated suicide gene therapy using nano/microbubbles and ultrasound. *Ultrasound Med Biol* 2008; **34**: 425–34.
22 Kodama T, Doukas AG, Hamblin MR. Delivery of ribosome-inactivating protein toxin into cancer cells with shock waves. *Cancer Lett* 2003; **189**: 69–75.
23 Kodama T, Hamblin MR, Doukas AG. Cytoplasmic molecular delivery with shock waves: importance of impulse. *Biophys J* 2000; **79**: 1821–32.
24 Kodama T, Tan PH, Offiah I *et al*. Delivery of oligodeoxynucleotides into human saphenous veins and the adjunct effect of ultrasound and microbubbles. *Ultrasound Med Biol* 2005; **31**: 1683–91.
25 Kojima H, Endo K, Moriyama H *et al*. Abrogation of mitochondrial cytochrome *c* release and caspase-3 activation in acquired multidrug resistance. *J Biol Chem* 1998; **273**: 16 647–50.
26 Abraham MC, Shaham S. Death without caspases, caspases without death. *Trends Cell Biol* 2004; **14**: 184–93.
27 Cemazar M, Miklavcic D, Mir LM *et al*. Electrochemotherapy of tumours resistant to cisplatin: a study in a murine tumour model. *Eur J Cancer* 2001; **37**: 1166–72.
28 Duvshani-Eshet M, Adam D, Machluf M. The effects of albumin-coated microbubbles in DNA delivery mediated by therapeutic ultrasound. *J Control Release* 2006; **112**: 156–66.
29 Taniyama Y, Tachibana K, Hiraoka K *et al*. Local delivery of plasmid DNA into rat carotid artery using ultrasound. *Circulation* 2002; **105**: 1233–9.
30 Koshiyama K, Kodama T, Yano T, Fujikawa S. Structural change in lipid bilayers and water penetration induced by shock waves: molecular dynamics simulations. *Biophys J* 2006; **91**: 2198–205.
31 Lee S, Anderson T, Zhang H, Flotte TJ, Doukas AG. Alteration of cell membrane by stress waves *in vitro*. *Ultrasound Med Biol* 1996; **22**: 1285–93.
32 Barlogie B, Corry PM, Drewinko B. *In vitro* thermochemotherapy of human colon cancer cells with cis-dichlorodiammineplatinum (II) and mitomycin C. *Cancer Res* 1980; **40**: 1165–8.
33 Weiss N, Delius M, Gambihler S, Eichholtz-Wirth H, Dirschedl P, Brendel W. Effect of shock waves and cisplatin on cisplatin-sensitive and – resistant rodent tumors *in vivo*. *Int J Cancer* 1994; **58**: 693–9.
34 Worle K, Steinbach P, Hofstadter F. The combined effects of high-energy shock waves and cytostatic drugs or cytokines on human bladder cancer cells. *Br J Cancer* 1994; **69**: 58–65.
35 Kambe M, Ioritani N, Shirai S *et al*. Enhancement of chemotherapeutic effects with focused shock waves: extracorporeal shock wave chemotherapy (ESWC). *In Vivo* 1996; **10**: 369–75.
36 Yu T, Huang X, Jiang S, Hu K, Kong B, Wang Z. Ultrastructure alterations in adriamycin-resistant and cisplatin-resistant human ovarian cancer cell lines exposed to nonlethal ultrasound. *Int J Gynecol Cancer* 2005; **15**: 462–7.
37 Siddik ZH. Cisplatin: mode of cytotoxic action and molecular basis of resistance. *Oncogene* 2003; **22**: 7265–79.
38 Honda H, Zhao QL, Kondo T. Effects of dissolved gases and an echo contrast agent on apoptosis induced by ultrasound and its mechanism via the mitochondria–caspase pathway. *Ultrasound Med Biol* 2002; **28**: 673–82.
39 Lagneaux L, de Meulenaer EC, Delforge A *et al*. Ultrasonic low-energy treatment: a novel approach to induce apoptosis in human leukemic cells. *Exp Hematol* 2002; **30**: 1293–301.
40 Li Y, Cohen R. Caspase inhibitors and myocardial apoptosis. *Int Anesthesiol Clin* 2005; **43**: 77–89.
41 Abdollahi A, Domhan S, Jenne JW *et al*. Apoptosis signals in lymphoblasts induced by focused ultrasound. *FASEB J* 2004; **18**: 1413–14.
42 Haag P, Frauscher F, Gradl J *et al*. Microbubble-enhanced ultrasound to deliver an antisense oligodeoxynucleotide targeting the human androgen receptor into prostate tumours. *J Steroid Biochem Mol Biol* 2006; **102**: 103–13.
43 Bekeredjian R, Kuecherer HF, Kroll RD, Katus HA, Hardt SE. Ultrasound-targeted microbubble destruction augments protein delivery into testes. *Urology* 2007; **69**: 386–9.
44 Armstrong DK, Bundy B, Wenzel L *et al*. Intraperitoneal cisplatin and paclitaxel in ovarian cancer. *N Engl J Med* 2006; **354**: 34–43.
45 Suzuki R, Takizawa T, Negishi Y *et al*. Gene delivery by combination of novel liposomal bubbles with perfluoropropane and ultrasound. *J Control Release* 2007; **117**: 130–6.
46 Tartis MS, McCallan J, Lum AF *et al*. Therapeutic effects of paclitaxel-containing ultrasound contrast agents. *Ultrasound Med Biol* 2006; **32**: 1771–80.
47 Rychak JJ, Klibanov AL, Hossack JA. Acoustic radiation force enhances targeted delivery of ultrasound contrast microbubbles: *in vitro* verification. *IEEE Trans Ultrason Ferroelectr Freq Control* 2005; **52**: 421–33.
48 Feril LB Jr, Kondo T. Biological effects of low intensity ultrasound: the mechanism involved, and its implications on therapy and on biosafety of ultrasound. *J Radiat Res (Tokyo)* 2004; **45**: 479–89.

厚生労働科学研究費補助金

第３次対がん総合戦略研究事業

新戦略に基づく抗がん剤の開発に関する研究

平成２０年度　総括・分担研究報告書

研究代表者　松村　保広

平成２１（２００９）年　３月

2/2冊

Journal of Controlled Release 133 (2009) 245–251

Contents lists available at ScienceDirect

Journal of Controlled Release

journal homepage: www.elsevier.com/locate/jconrel

Enhanced photodynamic cancer treatment by supramolecular nanocarriers charged with dendrimer phthalocyanine

Nobuhiro Nishiyama [a,1], Yoshinori Nakagishi [d,e,1], Yuji Morimoto [f,*], Ping-Shan Lai [g], Kozo Miyazaki [a,f], Kyoko Urano [a,f], Souta Horie [a], Michiaki Kumagai [a], Shigeto Fukushima [a], Yu Cheng [b], Woo-Dong Jang [h], Makoto Kikuchi [d], Kazunori Kataoka [a,b,c,*]

[a] Center for Disease Biology and Integrative Medicine, Graduate School of Medicine, The University of Tokyo, Tokyo, Japan
[b] Department of Materials Engineering, Graduate School of Engineering, The University of Tokyo, Tokyo, Japan
[c] Center for Nano-Bio Integration, The University of Tokyo, Tokyo, Japan
[d] Department of Medical Engineering, National Defense Medical College, Saitama, Japan
[e] Department of Surgery II, National Defense Medical College, Saitama, Japan
[f] Department of Integrative Physiology and Bio-Nano Medicine, National Defense Medical College, Saitama, Japan
[g] Department of Chemistry, Center of Nanoscience and Nanotechnology, National Chung-Hsing University, Taiwan
[h] Department of Chemistry, College of Science, Yonsei University, Seoul, Republic of Korea

ARTICLE INFO

Article history:
Received 1 August 2008
Accepted 6 October 2008
Available online 26 October 2008

Keywords:
Photodynamic therapy
Phthalocyanine
Dendrimer
Polymeric micelle

ABSTRACT

Photodynamic therapy (PDT) is a promising method for the localized treatment of solid tumors. In order to enhance the efficacy of PDT, we have recently developed a novel class of photosensitizer formulation, i.e., the dendrimer phthalocyanine (DPc)-encapsulated polymeric micelle (DPc/m). The DPc/m induced efficient and unprecedentedly rapid cell death accompanied by characteristic morphological changes such as blebbing of cell membranes, when the cells were photoirradiated using a low power halogen lamp or a high power diode laser. The fluorescent microscopic observation using organelle-specific dyes demonstrated that DPc/m might accumulate in the endo-/lysosomes; however, upon photoirradiation, DPc/m might be promptly released into the cytoplasm and photodamage the mitochondria, which may account for the enhanced photocytotoxicity of DPc/m. This study also demonstrated that DPc/m showed significantly higher *in vivo* PDT efficacy than clinically used Photofrin® (polyhematoporphyrin esters, PHE) in mice bearing human lung adenocarcinoma A549 cells. Furthermore, the DPc/m-treated mice did not show skin phototoxicity, which was apparently observed for the PHE-treated mice, under the tested conditions. These results strongly suggest the usefulness of DPc/m in clinical PDT.

1. Introduction

Photodynamic therapy (PDT), an effective modality for treating localized tumors, involves the systemic administration of porphyrin- or phthalocyanine-based photosensitizers (PSs), followed by local photoirradiation of solid tumors with the light of a specific wavelength [1–3]. Upon photoirradiation, PSs generate reactive oxygen species (ROS) such as singlet oxygen, leading to photochemical destruction of tumor vessels and tumor tissues. PDT shows a high clinical complete response to early-stage superficial tumors, including lung, esophageal, gastric, and cervical cancers. Also, PDT is quite useful as an initial treatment for malignant tumors because organ functions are maintained, thus saving the patient's stamina for further treatments. However, PDT is known to be accompanied by skin hyperphotosensitivity, so that the patient needs to stay in a darkened room for at least 2 weeks. This effect is attributable to the lack of tumor selectivity by currently approved PSs, such as Photofrin® [3]. Tumor-selective PSs and their formulations are expected to restrain unfavorable side effects and improve the efficacy of PDT against intractable tumors. In this context, the use of long-circulating nanocarriers such as liposomes [4], water-soluble polymers [5–7] and polymeric micelles [8–10] is a promising way to improve the tumor selectivity of PSs. It has been demonstrated that such nanocarriers can preferentially and effectively accumulate in solid tumors, since the tumor tissues are characterized by the enhanced permeability and retention (EPR) effect, which consists of microvascular hyperpermeability to circulating macromolecules and impaired lymphatic drainage [11].

* Corresponding authors. Morimoto is to be contacted at the Department of Integrative Physiology and Bio-Nano Medicine, National Defense Medical College, Namiki 3-2, Tokorozawa, Saitama 359-8513, Japan. Tel.: +81 4 2995 1482; fax: +81 4 2996 5187. Kataoka, Department of Materials Engineering, Graduate School of Engineering, The University of Tokyo, 7-3-1 Hongo, Bunkyo-ku, Tokyo 113-8656, Japan. Tel.: +81 3 5841 7138; fax: +81 3 5841 7139.
E-mail addresses: moyan@ndmc.ac.jp (Y. Morimoto), kataoka@bmw.t.u-tokyo.ac.jp (K. Kataoka).
[1] These authors contributed equally to this work.

0168-3659/$ – see front matter © 2008 Elsevier B.V. All rights reserved.
doi:10.1016/j.jconrel.2008.10.010

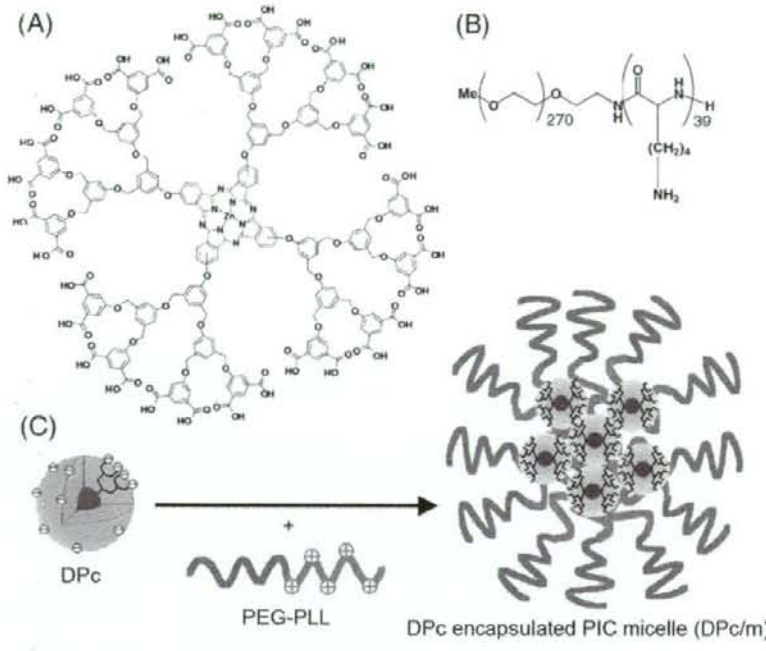

Fig. 1. Chemical structures of anionic dendrimer phthalocyanine (DPc) (A) and poly(ethylene glycol)–poly(L-lysine) (PEG–PLL) block copolymer (B). The DPc-encapsulated polyion complex (PIC) micelle (DPc/m) was formed by mixing DPc and PEG–PLL at a charge stoichiometric ratio (C).

Regarding the development of nanocarriers encapsulating PSs, most conventional PSs may have several serious drawbacks. Since potent PSs generally have large π-conjugation domains, they easily form aggregates due to their π–π and hydrophobic interactions. Such aggregate formation severely decreases the ROS formation essential to the PDT effect [12,13]. Also, this propensity may hamper the encapsulation of PSs into nanocarriers such as liposomes and polymeric micelles. To solve such problems, we have developed ionic dendrimer photosensitizers where the core of porphyrin or phthalocyanine is surrounded by large dendritic wedges [14,15]. Unlike conventional PSs, dendrimer photosensitizers exhibit effective ROS production even at extremely high concentrations, because the dendritic wedges sterically prevent or weaken aggregation of the center dye molecules [13,16]. In addition, ionic groups on the peripheries of dendrimer photosensitizers allow their stable incorporation into polyion complex (PIC) micelles through the electrostatic interaction with oppositely charged poly(ethylene glycol)(PEG)–polyelectrolyte block copolymers [10,13,15,16]. Polymeric micelles, which are characterized by a size of several tens of nanometers and a core–shell architecture, are potent nanocarriers for site-specific drug delivery, as several formulations encapsulating antitumor agents have already progressed to clinical studies [17–19]. We have already demonstrated that PIC micelles encapsulating third-generation dendrimer porphyrin showed remarkably high photocytotoxicity against cancer cells and successfully treated experimental disease models of choroidal neovascularization (CNV) in rats [20], indicating that dendrimer photosensitizer-encapsulated PIC micelles show great promise for use in clinical PDT.

Recently, we prepared PIC micelles through the electrostatic interaction between the anionic dendrimer phthalocyanine (DPc) and the PEG–poly(L-lysine) block copolymer (PEG–PLL) (Fig. 1) [15]. Since DPc has strong Q-band absorption at 685 nm, at which the light deeply penetrates tissues, the DPc-encapsulated PIC micelle (DPc/m) is assumed to be effective in PDT of solid tumors. In our previous paper, DPc/m showed approximately three- to four-fold decrease in the oxygen consumption rate compared with free DPc, indicating a decrease in quantum yield of singlet oxygen formation [15]. Compared with aforementioned dendrimer porphyrin, a relatively small dendritic wedge of DPc may not entirely prevent collisional quenching in the micellar core. Nevertheless, DPc/m displayed approximately 100-fold higher *in vitro* photocytotoxicity against human cervical cancer HeLa cells compared with free DPc when the cells were photoirradiated for 60 min with broad-band light (400–700 nm) using a low power halogen lamp [15]. However, the underlying mechanisms of the enhanced photocytotoxicity of DPc/m remain to be clarified yet, because DPc/m showed only 4 times higher cellular uptake compared with free DPc. In the present paper, we have studied *in vitro* photocytotoxicity of DPc/m when human lung adenocarcinoma A549 cells were photoirradiated by a diode laser (670 nm), and found that DPc/m showed unique photochemical processes inside of the cells to induce cell death in an unprecedentedly fast manner. Also, we have studied *in vivo* antitumor activity of DPc/m against subcutaneous tumor models in mice.

2. Materials and Methods

2.1. Preparation of DPc and DPc/m

The synthesis of anionic dendrimer phthalocyanine (DPc) has been reported previously [15,21]. The synthesized DPc is composed of the 2nd generation aryl ether dendrimer with a Zn(II)-phthalocyanine center and 32 carboxylic groups on its periphery (Fig. 1A). Poly (ethylene glycol)–poly(L-lysine) block copolymer (PEG–PLL) (Fig. 1B) was synthesized by the polymerization of the *N*-carboxy anhydride of N^{ε}-Z-L-lysine initiated by CH_3O-PEG-NH_2 (12,000 g/mol), followed by deprotection of the Z group according to a previously reported method [22]. The polymerization degree of PLL segment was determined to be 39 by the ^{1}H NMR measurement. The DPc-encapsulated PIC micelle (DPc/m) was prepared at a charge stoichiometric ratio of negatively-charged DPc and positively-charged PEG–

PLL (Fig. 1C). The resulting DPc/m had a diameter of ca. 50 nm with a narrow size distribution (unimodal, $\mu_2/\Gamma^2 = 0.12$) and zeta-potential value of −0.56±0.56 mV, which were measured by a Zetasizer nanoseries (Malvern Instruments Ltd., UK).

2.2. Cell culture and cytotoxicity assay

Human lung adenocarcinoma A549 cells were obtained from Riken Bioresource Center Cell Bank (Tsukuba, Japan). A549 cells were maintained in Dulbecco's modified Eagle medium (Invitrogen, Carlsbad, CA) containing 10% fetal bovine serum in a humidified atmosphere containing 5% CO_2 at 37 °C. The light-induced cytotoxicity (photocytotoxicity) of each photosensitizing agent was evaluated as follows: In a darkened room, the cells were incubated with photosensitizing agents for 24 h. After washing with PBS and medium replacement, the cells were photoirradiated using a low power halogen lamp or a high power diode laser. In the former case, the culture plate was irradiated with broad-band visible light using a halogen lamp equipped with a filter passing light of 400–700 nm (fluence rate: 3.0 mW/cm^2; irradiation time: 15, 30, 45, and 60 min; fluence: 2.7–10.8 J/cm^2). In the latter case, each well was photoirradiated by a 670 nm, continuous wave diode laser (HLD2000MT 7A, High Power Devices, North Brunswick, NJ) (fluence rates: 25, 50, and 100 mW/cm^2; irradiation time: 1000 s; fluence: 25–100 J/cm^2). The cell viability was evaluated by MTT assay 24 h after photoirradiation.

2.3. Observation of morphological changes of the cell during photoirradiation

To investigate the modality of light-induced cell death, we examined the morphological changes occurring in DPc- and DPc/m-treated cells during photoirradiation in a time-lapse manner. In this experiment, A549 cells were incubated with DPc or DPc/m for 24 h at the 99% cell growth-inhibitory concentration (IC_{99}). After the medium was replaced, the morphological changes in the cells during photoirradiation by the light source of a time-lapse sectioning fluorescent microscope (ApoTome/Axiovert 200 M, Carl Zeiss, Oberkochen, Germany; fluence rate: ~120 mW/cm^2) were continuously monitored using the microscope's differential interference contrast (DIC) mode. In addition, the fluorescent images from DPc and Rhodamine 123 (Rh123) (Molecular Probes, Eugene, OR), a specific dye to the mitochondria, were simultaneously observed.

2.4. Intracellular localization of DPc/m

To evaluate the intracellular localization of DPc/m, PEG–PLL was labeled with Alexa fluor 488 carboxylic acid, succinimidyl ester (5.0 mg, 7.8 μmol) (Invitrogen) according to the manufacturer's protocol. After removal of unbound dye by dialysis and lyophilization, the ratio of the dye to PEG–PLL was estimated to be 3.8 by measuring UV–Vis spectra. The Alexa 488-labeled DPc/m was prepared as above-mentioned.

Intracellular localization of Alexa 488-labeled DPc/m in A549 cells was observed by confocal laser scanning microscopy (CLSM) (LSM510META, Carl Zeiss). After 24-h incubation with Alexa 488-labeled DPc/m and subsequent washing, the cells were treated with LysoTracker Red DND-99, MitoTracker Red 580, and ER Tracker Red (Molecular Probes) for the staining of endo-/lysosomes, mitochondria, and endoplasmic reticulum, respectively. The fluorescent images of the cells without photoirradiation were observed by CLSM.

2.5. Measurement of ROS production in the mitochondria

The ROS production in the mitochondria in A549 cells was detected by MitoSOX Red reagent (Invitrogen), which rapidly accumulates in the mitochondria and exhibits fluorescence upon oxidation by superoxide and other ROS. After 24-h incubation with DPc or DPc/m, the cells were incubated with MitoSOX Red (5 μM) for 10 min at 37 °C. Then, the fluorescent image of MitoSOX Red in living cells during photoirradiation using the light source of the microscope was observed by CLSM (TCS SP2 Spectral Confocal System, Leica, Nussloch, Germany).

2.6. In vivo antitumor effect

The antitumor activity of DPc, DPc/m or Photofrin® (porfimer sodium, PHE from Wyeth, Madison, NJ) was tested against subcutaneous tumor models of A549 cells in mice ($n = 6$). A549 cells (3×10^6) were subcutaneously transplanted into the left back of 6-week-old female nude mice (BALB/c *nu/nu*) (Clea Japan, Tokyo, Japan). Fifteen days after transplantation, one of the photosensitizing agents was administered intravenously at a dose of 1.85 mg/kg (0.37 μmol/kg photosensitizing unit) for DPc and DPc/m and 1.65 mg/kg (2.7 μmol/kg photosensitizing unit) for PHE. Twenty-four hours after the administration, tumor sites were irradiated with a diode laser with a light dose of 100 J/cm^2. This animal study protocol was approved by the Ethics Committee for Laboratory Animals of the National Defense Medical College, Tokorozawa, Japan.

2.7. Skin phototoxicity

Six-week-old female nude mice (BALB/c *nu/nu*) were intravenously administered 4.2 μmol/kg DPc/m or 8.1 μmol/kg Photofrin® (PHE), followed by white light irradiation to abdominal skin using a halogen lamp at the fluence of 60 J/cm^2 at 0.5, 1, 2 or 4 days after administration. Four days after irradiation, macroscopic changes in the skin as well as in the organs were observed.

3. Results

3.1. In vitro PDT using halogen lamp

Table 1 summarizes the 50% cell growth inhibitory concentrations (IC_{50}) of DPc, DPc/m and Photofrin® (PHE) against A549 cells. Note that none of the photosensitizing agents showed dark toxicity. As shown in Table 1, DPc/m exhibited an irradiation time-dependent increase in cytotoxicity, which is consistent with our previous results of the photocytotoxicity against HeLa cells [14]. Eventually, DPc/m achieved 78-fold higher photocytotoxicity than free DPc at 10.8 J/cm^2. It is worth mentioning that DPc/m was 3.9 times more effective than even clinically used PHE on a molar basis of photosensitizing units.

3.2. In vitro PDT using diode laser

The photocytotoxicity of DPc and DPc/m against A549 cells are summarized in Table 2 and Fig. S1 in Supporting Information. As shown in Table 2, DPc/m exhibited 44-fold higher photocytotoxicity than DPc at 25 J/cm^2. It is noteworthy that DPc displayed a fluence-rate-dependent increase in photocytotoxicity, whereas DPc/m was

Table 1
In vitro cytotoxicity of photosensitizing agents after photoirradiation using halogen lamp

Photoirradiate condition		IC_{50} (μM)[a] of photosensitizing agent		
Time (min)	Fluence (J/cm^2)	DPc	DPc/m	PHE
0	0	N.D.[b]	N.D.	N.D.
15	2.7	N.D.	1.0	1.0
30	5.4	N.D.	0.20	0.60
45	8.1	N.D.	0.20	0.35
60	10.8	7.0	0.090	0.35

[a] 50% cell growth-inhibitory concentration.
[b] IC_{50} was higher than the highest examined concentration (20 μM).

Table 2
In vitro cytotoxicity of photosensitizing agents after photoirradiation using diode laser

Photoirradiate condition	IC_{50} (μM) of photosensitizing agent	
Fluence (J/cm^2)	DPc	DPc/m
25	20	0.45
50	4.8	0.16
100	0.86	0.11

less influenced by the fluence rate. Eventually, DPc/m showed only 7.9-fold higher photocytotoxicity than DPc at 100 J/cm^2.

3.3. Observation of morphological changes of the cell during photoirradiation

The morphological changes occurring in the DPc- and DPc/m-treated cells during photoirradiation were monitored in a time-lapse manner. The observations revealed marked differences between DPc and DPc/m (Fig. 2). The DPc/m-treated cells swelled rapidly, accompanied by membrane blebbing, resulting in the disappearance of the initial shape of the cells within a few minutes of photoirradiation. In contrast, the DPc-treated cells showed gradual shrinkage while maintaining their pseudopodial structures during photoirradiation.

In addition, the fluorescent images from DPc and Rh123, a specific dye to the mitochondria, were simultaneously monitored and are also shown in Fig. 2. Regarding the fluorescence from DPc (red), the DPc-treated cells exhibited a transient burst in the fluorescence: the fluoresce of DPc increased appreciably 60–180 s after the initiation of photoirradiation and became obscure within 400 s. Such unique behavior was also seen in the DPc/m-treated cells; however, the fluorescent burst occurred faster than DPc. On the other hand, there were characteristic differences in the Rh123 fluorescence (green). The Rh123 fluorescence in the DPc/m-treated cells disappeared immediately after the initiation of light irradiation. In contrast, the fluorescence of Rh123 in the DPc-treated cells remained even after 450 s photoirradiation. These results suggest that DPc/m might affect mitochondrial functions during photoirradiation, leading to rapid cell death with characteristic morphological changes.

3.4. Intracellular localization of DPc/m

The intracellular localization of DPc/m in A549 cells before photoirradiation was observed by CLSM. The fluorescence image in Fig. 3A reveals that Alexa 488-labeled DPc/m showed punctate fluorescence co-localized with LysoTracker Red DND-99. In contrast, the fluorescence pattern of Alexa 488-labeled DPc/m was apparently different from those of MitoTracker Red 580 and ER Tracker Red, as shown in Fig. 3B and C, respectively. We also observed the intracellular localization of DPc and DPc/m after 24-h incubation by utilizing DPc's fluorescence, and found that both of them were co-localized with LysoTracker Green DND-26 (Fig. S2 in Supporting Information). These results indicate that DPc and DPc/m may have been internalized through the endocytic pathway and may have localized in the endo-/lysosomes before photoirradiation.

3.5. Measurement of ROS production in the mitochondria

Since DPc/m is assumed to affect the mitochondria, as suggested in Fig. 2, we evaluated ROS production in the mitochondria of A549 cells using MitoSOX Red. As shown in Fig. 4, MitoSOX Red exhibited apparent fluorescence in the DPc/m-treated cells after 1 min photoirradiation, whereas no appreciable fluorescence appeared in the DPc-treated cells even after prolonged photoirradiation. Thus, DPc/m might induce photodamage to the mitochondria and thus affect their functions.

3.6. In vivo antitumor effect and skin phototoxicity

The mice bearing subcutaneous A549 tumors were treated with the PDT using DPc, DPc/m or Photofrin® (PHE), and the relative tumor volumes after photoirradiation are shown in Fig. 5. As a result, the tumors in the DPc/m-treated mice grew significantly slower than those in the DPc-treated mice. It is worth mentioning that the PDT effect of DPc/m was superior to that of PHE, although the injected dose of DPc/m was 7.3-fold lower than that of PHE on the basis of photosensitizing units. On the other hand, we also evaluated *in vivo* phototoxicity after PDT. As shown in Fig. 6B, severe damage to the skin and liver was observed in PHE-administered mice (8.1 μmol/kg photosensitizing unit). In contrast, DPc/m did not induce such damage, although a relatively high dose of DPc/m (4.2 μmol/kg photosensitizing unit) was administered in this study (Fig. 6A). Thus, DPc/m was demonstrated to be a safe but effective photosensitizer formulation over clinically used PHE.

4. Discussion

The targeted delivery of PSs using nanocarriers such as liposomes and polymeric micelles have been studied to improve the therapeutic efficacy and restrain side effects in PDT [4–10,13–16]. The use of nanocarriers is expected to increase the concentration of PSs in the tumor tissue based on the EPR effect [10]; however, incorporation of

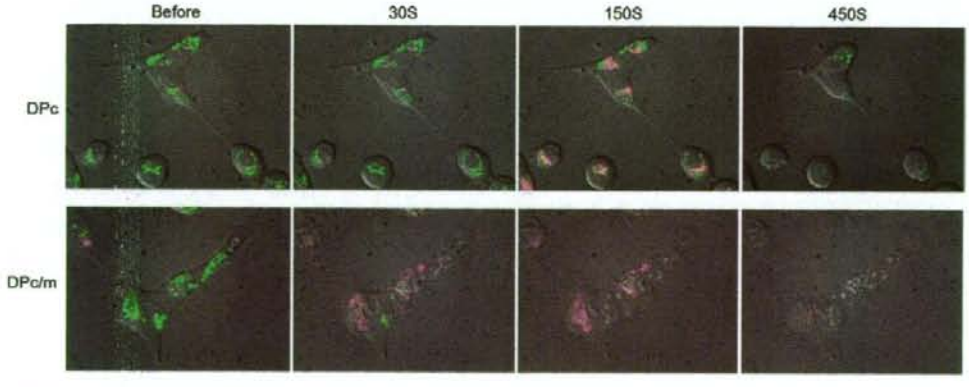

Fig. 2. Time-dependent morphological changes of the DPc- and DPc/m-treated A549 cells during photoirradiation. The fluorescences from DPc (red) and Rhodamine 123 (Rh123) (green) were simultaneously monitored.

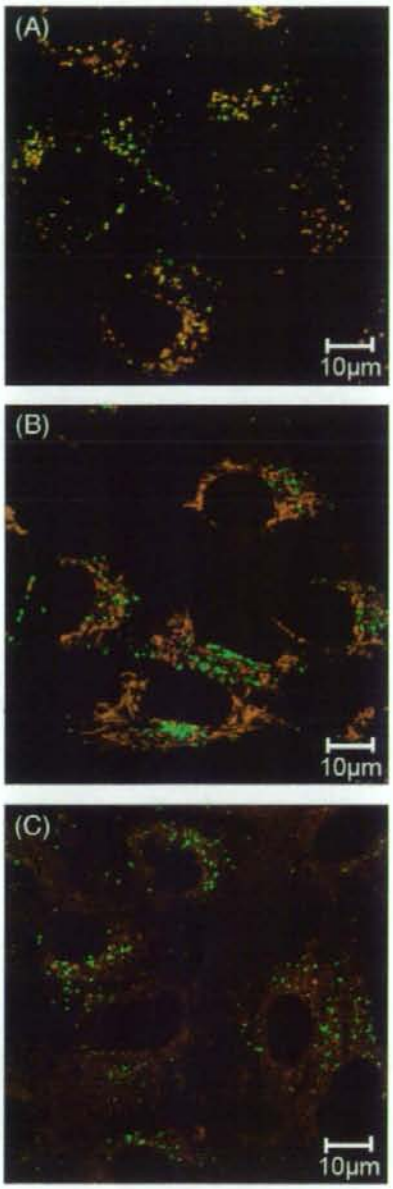

Fig. 3. Intracellular localization of Alexa488-labeled DPc/m (green) in A549 cells without photoirradiation. The cells were stained with LysoTracker Red DND-99 (red) for staining the lysosomes (A), MitoTracker Red 580 (red) for staining the mitochondria (B) and ER Tracker Red for staining endoplasmic reticulum (ER) (C).

PSs into nanocarriers generally decreases the singlet oxygen quantum yield due to the concentration quenching of PSs, leading to considerable reduction of photocytotoxicity [12,13]. In this study, we demonstrated that our unique photosensitizer–nanocarrier combination, i.e., dendrimer phthalocyanine (DPc)-encapsulated polymeric micelles (DPc/m), showed remarkably enhanced photocytotoxicity over free DPc, and achieved significantly higher *in vitro* and *in vivo* PDT effect compared with clinically used Photofrin® (PHE). Therefore, we also focused on the underlying mechanisms of the efficient photo-induced cell death by DPc/m.

In Table 1, DPc/m showed 78-fold higher photocytotoxicity than free DPc. Such remarkable enhancement of DPc/m's photocytotoxicity cannot be explained by the intracellular concentration of DPc: DPc/m exhibited only 7.6-fold higher cellular uptake than free DPc in A549 cells (data not shown). In addition, we previously demonstrated that DPc/m showed an approximately three- to fourfold slower oxygen consumption rate compared with free DPc [15]. We therefore assume that different mechanisms may underlie photo-induced cell death between DPc/m and free DPc. In the present paper, we also studied the effect of photoirradiation by a high-power diode laser on photocytotoxicity. As a result, there were considerable differences in the fluence-rate-dependency of photocytotoxicity between DPc and DP/m (Table 2). Meanwhile, we have also studied the time-dependent morphological changes of the cells during PDT, and found marked differences between DPc and DPc/m (Fig. 2). The DPc/m induced unprecedentedly rapid cell death accompanied by characteristic morphological changes including swelling and membrane blebbing. Note that such characteristic morphological changes in the DPc/m-treated cells appear to be similar to the characteristics of *oncosis*, which is reported to be induced by several pathological conditions, such as hypoxia, inhibition of ATP production, and increased permeability of the plasma membrane [23].

To further study unique light-induced cell death by DPc/m, we have studied intracellular localization of DPc/m. We observed that both DPc and DPc/m selectively accumulated in the endo-/lysosomes, suggesting their cellular internalization through the endocytosis (Fig. 3 and Fig. S2). However, once the cells were photoirradiated, the DPc and DPc/m may have been translocated from the endo-/lysosomes to the

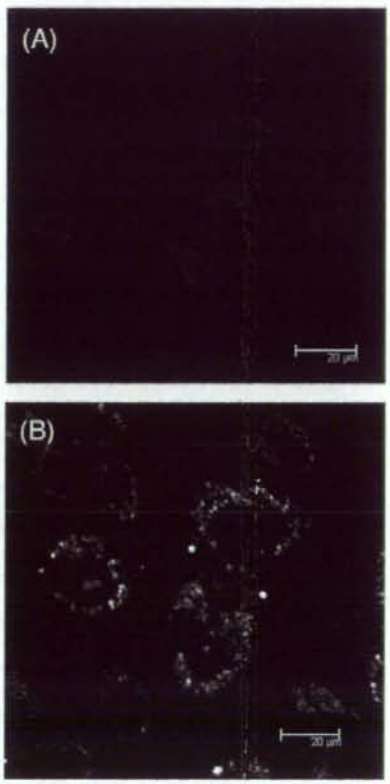

Fig. 4. Fluorescence of MitoSOX Red in the DPc- (A) and DPc/m (B)-treated A549 cells after 1 min photoirradiation.

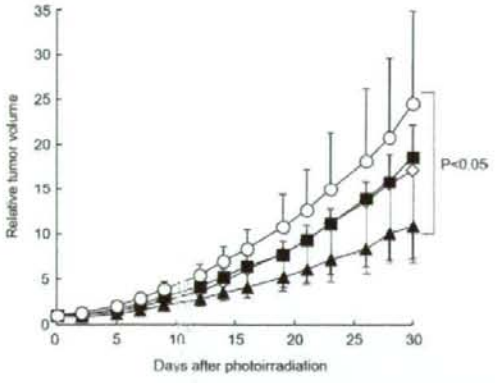

Fig. 5. Growth curves of subcutaneous A549 tumors in control mice (open circle) and mice administered with 0.37 μmol/kg DPc (closed square), 0.37 μmol/kg DPc/m (closed triangle) and 2.7 μmol/kg Photofrin® (PHE) (open diamond) ($n=6$). Twenty-four hours after administration of photosensitizing agents, the tumors were photoirradiated using a diode laser (fluence: 100 J/cm^2).

cytoplasm, because DPc fluorescence became apparent in a diffusive manner in both the DPc- and DPc/m-treated cells (Fig. 2). The mechanism of this translocation is the photochemical disruption of the endo-/lysosomal membranes: this is called photochemical internalization (PCI), a new concept for light-induced cytoplasmic delivery of cell-membrane-impermeable low-molecular-weight drugs as well as macromolecular compounds, such as nucleic acids and proteins [24,25]. In our previous papers, we indeed demonstrated that DPc and DPc/m allowed the efficient endosomal escape of non-viral gene vectors, achieving light-induced and site-directed transfection *in vitro* and *in vivo* [27,28]. Possibly, the increased fluorescence of DPc/m in Fig. 2 may reflect the destabilization of the micellar structure due to photochemical reactions: this destabilization may be essential to the interaction of DPc/m with the endo-/lysosomal membranes.

It is known that the efficiency of light-induced cell death in PDT depends on which sites in the cell are photodamaged [2,3]. In this regard, photodamage to the mitochondria could induce efficient cell death, whereas endo-/lysosomes are less susceptible to photocytotoxicity [3]. Therefore, we focused on the effects of PDT using DPc/m on the mitochondria. In Fig. 2, we evaluated the time-dependent changes in the fluorescence of Rh123, a specific dye to the mitochondria, during photoirradiation in PDT using DPc or DPc/m. The fluorescence of Rh123 in the DPc/m-treated cells immediately disappeared after the initiation of photoirradiation, whereas that in the DPc-treated cells remained even after 450 s photoirradiation. Note that the fluorescent intensity of Rh123 is correlated with the amount of ATP in the cells [28]. Therefore, it is assumed that DPc/m might directly or indirectly clip the ATP in the cell. To clarify whether the effects of DPc/m on the mitochondrial functions are attributed to its direct photodamage to the mitochondria or not, we detected the ROS production in the mitochondria by using MitoSOX Red (Fig. 4). As a result, only DPc/m showed appreciable ROS production in the mitochondria upon photoirradiation. These results suggest that DPc/m might induce photodamage to the mitochondria and thus affect their functions.

Based on all the aforementioned results, DPc and DPc/m are assumed to undergo the following steps in the photo-induced cell death. (i) DPc and DPc/m are internalized through the endocytic pathway and accumulate in the endo-/lysosomes. In this step, DPc/m showed 7.6-fold higher cellular uptake than free DPc. (ii) Upon photoirradiation, DPc and DPc/m are translocated from the endo-/lysosomes to the cytoplasm through the photochemical disruption of the endo-/lysosomal membranes. We previously reported that DPc/m is more efficient than DPc in the PCI-mediated gene transfection [26]. (iii) Only DPc/m might accumulate in the mitochondria and produce the ROS, resulting in exhaustion of ATP in the cell. In contrast, DPc showed no ROS production in the mitochondria. These steps may account for DPc/m's much higher photocytotoxicity compared to DPc. Also, PDT using DPc/m induced unique cell death, similar to a characteristic of *oncosis*. The photodamage to the mitochondria and/or the exhaustion of intracellular ATP may be attributed to this unique cell death by DPc/m. In addition to the subcellular localization of DPc/m and the photodamaged sites in the cell, the characteristic structure of DPc/m, in which several tens DPc molecules are concentrated in a 50 nm nanocontainer, may also contribute to the remarkably high photocytotoxicity. Note that DPc/m from PEG–PLL with the polymerization degree of PLL of 43 contained 77 DPc molecules in the core (Fig. S3 in Supporting Information). The high local concentration of DPc within the micellar core is assumed to generate a high concentration of ROS at a local site, achieving a high photochemical oxidation level that exceeds the threshold of cell death. Note that, in the case of other nanocarriers containing conventional PSs, it may be difficult to achieve such a high local concentration of ROS due to the concentration quenching of PSs [13]. Furthermore, although ROS, especially singlet oxygen, have very short half-lives (~2 μs) in aqueous media [3], a high local concentration of ROS achieved by DPc/m may allow the oxidization of the greater regions in the cell. Such effects of spatially regulated incorporation of PSs into nanocarriers on PDT are quite intriguing, and further studies should be performed.

In this study, we also demonstrated that DPc/m showed significantly higher *in vivo* antitumor activity against subcutaneous A549 tumors compared with clinically used PHE, although the injected dose of DPc/m was 7.3-fold lower than that of PHE on the basis of photosensitizing units (Fig. 5). This superior effect may be explained by the effective accumulation of DPc/m based on the EPR effect and its enhanced photocytotoxicity, as mentioned above. In general, *in vivo* PDT effect is known to be very complicated and can be affected by several parameters, including accumulation and penetrability of

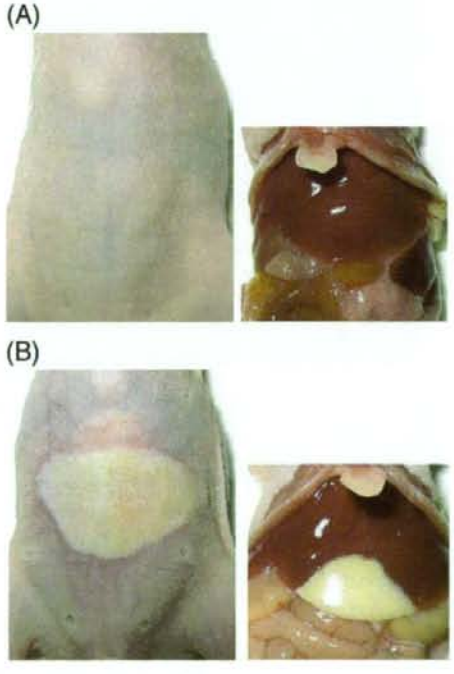

Fig. 6. Macroscopic observation of the skin and organs in the mice treated with 4.2 μmol/kg DPc/m (A) and 8.1 μmol/kg Photofrin® (PHE) (B) at 4 days after light irradiation to abdominal skin using a halogen lamp (fluence: 60 J/cm^2).

photosensitizers (PSs) in the tumor tissue, possible targets (i.e., tumor vasculature and cancer cells), and tissue penetration of light [1]; therefore, there may be a room for further improvement in the *in vivo* efficacy. In this regard, we are going to study the mechanism of *in vivo* PDT effect by DPc/m, optimizing several factors to maximize the therapeutic effect in the near future. Importantly, the PHE-administered mice showed severe damages to the skin and liver after exposure to white light; however, the DPc/m-administered mice did not show such side effects regardless of the injected dose (Fig. 6). These results may be attributed to the reduced accumulation of DPc/m in the skin and normal organs. In general, the skin phototoxicity might result from non-specific accumulation of conventional PSs in the skin, because they could penetrate the endothelium and eventually accumulate in various organs and tissues. In contrast, nanocarriers or macromolecular photosensitizers are assumed not to pass through the tight junctions of the vasculature in the tissues except for the liver, spleen, and tumor, which possess leaky vasculatures. Therefore, it is assumed that nanocarriers or macromolecular photosensitizers may not accumulate in the skin, thus preventing skin phototoxicity. Furthermore, no skin damage was found after photoirradiation even at 1 h after DPc/m administration (data not shown). Possibly, DPc/m in the bloodstream may not be photoactivated by light irradiation, owing to strong absorption by a heme in red blood cells.

5. Conclusion

The DPc/m elicited remarkably effective and rapid light-induced cell death. Following internalization by endocytosis, DPc/m seemed to be translocated from the endo-/lysosomes to the cytoplasm during photoirradiation and subsequently induce photodamage to the mitochondria. Such unique intracellular localization of DPc/m may be responsible for the enhanced photocytotoxicity mentioned above. In animal experiments, DPc/m showed significantly higher antitumor activity than clinically used PHE. Furthermore, unlike the PHE-treated mice, the DPc/m-treated mice showed no sign of skin phototoxicity. Thus, DPc/m is expected to serve as an innovative photosensitizer formulation to improve the effectiveness and safety of current PDT.

Acknowledgment

This study was supported by the New Energy and Industrial Technology Development Organization (NEDO) of Japan (project code: P06042).

Appendix A. Supplementary data

Supplementary data associated with this article can be found, in the online version, at doi:10.1016/j.jconrel.2008.10.010.

References

[1] D.E.J.G.J. Dolmans, D. Fukumura, R.K. Jain, Photodynamic therapy for cancer, Nat. Rev. Cancer 3 (5) (2003) 380–387.
[2] T.J. Dougherty, C.J. Gomer, B.W. Henderson, G. Jori, D. Kessel, M. Korbelik, J. Moan, Q. Peng, Photodynamic therapy, J. Natl. Cancer Inst. 90 (12) (1998) 889–905.
[3] I.J. Macdonald, T.J. Dougherty, Basic principles of photodynamic therapy, J. Porphyr. Phthalocyanines 5 (2) (2001) 105–129.
[4] A.S.L. Derycke, P.A.M. de Whitte, Liposomes for photodynamic therapy, Adv. Drug Deliv. Rev. 56 (1) (2004) 17–30.
[5] J.G. Shiah, Y. Sun, M. Peterson, R.C. Straight, J. Kopecek, Antitumor activity of N-(2-hydroxypropyl)methacrylamide copolymer-mesochlorine$_{e_6}$ and adriamycin conjugates in combination treatments, Clin. Cancer Res. 6 (3) (2000) 1008–1015.
[6] M.R. Hamblin, J.L. Miller, I. Rizvi, B. Ortel, E.V. Maytin, T. Hasan, Pegylation of a chlorine6 polymer conjugate increases tumor targeting of photosensitizer, Cancer Res. 61 (19) (2001) 7155–7162.
[7] C. Kojima, Y. Toi, A. Harada, K. Kono, Preparation of poly(ethylene glycol)-attached dendrimers encapsulating photosensitizers for application to photodynamic therapy, Bioconjug. Chem. 18 (3) (2007) 663–670.
[8] C.F. van Nostrum, Polymeric micelles to deliver photosensitizers for photodynamic therapy, Adv. Drug Deliv. Rev. 56 (1) (2004) 9–16.
[9] D. Le Garrec, J. Taillefer, J.E. Van Lier, V. Lenaerts, J.-C. Leroux, Optimizing pH-responsive polymeric micelles for drug delivery in a cancer photodynamic therapy model, J. Drug Target. 10 (5) (2002) 429–437.
[10] H.R. Stapert, N. Nishiyama, D.L. Jiang, T. Aida, K. Kataoka, Polyion complex micelles encapsulating light-harvesting ionic dendrimer zinc porphyrins, Langmuir 16 (21) (2000) 8182–8188.
[11] Y. Matsumura, H. Maeda, A new concept for macromolecular therapeutics in cancer chemotherapy: mechanism of tumoritropic accumulation of proteins and the antitumor agent SMANCS, Cancer Res. 46 (12) (1986) 6387–6392.
[12] N. Cauchon, H. Tian, R. Langlois, C. La Madeleine, S. Martin, H. Ali, D. Hunting, J.E. van Lier, Structure-photodynamic activity relationships of substituted zinc trisulfophthalocyanines, Bioconjug. Chem. 16 (1) (2005) 80–89.
[13] Y. Li, W.-D. Jang, N. Nishiyama, A. Kishimura, S. Kawauchi, Y. Morimoto, S. Miake, T. Yamashita, M. Kikuchi, T. Aida, K. Kataoka, Dendrimer generation effects on photodynamic efficacy of dendrimer porphyrins and dendrimer-loaded supramolecular nanocarriers, Chem. Mater. 19 (23) (2007) 5557–5562.
[14] N. Nishiyama, H.R. Stapert, G.D. Zhang, D. Takasu, D.L. Jiang, T. Nagano, T. Aida, K. Kataoka, Light-harvesting ionic dendrimer porphyrins as new photosensitizers for photodynamic therapy, Bioconjug. Chem. 14 (1) (2003) 58–66.
[15] W.-D. Jang, Y. Nakagishi, N. Nishiyama, S. Kawauchi, Y. Morimoto, M. Kikuchi, K. Kataoka, Polyion complex micelle for photodynamic therapy: incorporation of dendritic photosensitizer excitable at long wavelength relevant to improved tissue-penetrating property, J. Control. Release 113 (1) (2006) 73–79.
[16] W.-D. Jang, N. Nishiyama, G.D. Zhang, A. Harada, D.-L. Jiang, S. Kawauci, Y. Morimoto, M. Kikuchi, H. Koyama, T. Aida, K. Kataoka, Supramolecular nanocarrier of anionic dendrimer porphyrins with cationic block copolymers modified with polyethylene glycol to enhance intracellular photodynamic efficacy, Angew. Chem., Int. Ed. 44 (3) (2005) 419–423.
[17] N. Nishiyama, S. Okazaki, H. Cabral, M. Miyamoto, Y. Kato, Y. Sugiyama, K. Nishio, Y. Matsumura, K. Kataoka, Novel cisplatin-incorporated polymeric micelles can eradicate solid tumors in mice, Cancer Res. 63 (24) (2003) 8977–8983.
[18] K. Kataoka, A. Harada, Y. Nagasaki, Block copolymer micelles for drug delivery: design, characterization and biological significance, Adv. Drug Deliv. Rev. 47 (1) (2001) 113–131.
[19] N. Nishiyama, K. Kataoka, Current state, achievements, and future prospects of polymeric micelles as nanocarriers for drug and gene delivery, Pharmacol. Ther. 112 (3) (2006) 630–648.
[20] R. Ideta, F. Tasaka, W.-D. Jang, N. Nishiyama, G.-D. Zhang, A. Harada, Y. Yanagi, Y. Tamaki, T. Aida, K. Kataoka, Nanotechnology-based photodynamic therapy for neovascular disease using a supramolecular nanocarrier loaded with a dendritic photosensitizer, Nano Lett. 5 (12) (2005) 2426–2431.
[21] Z. Sheng, X. Ye, Z. Zheng, S. Yu, D.K.P. Ng, T. Ngai, C. Wu, Transient absorption and fluorescence studies of disstacking phthalocyanine by poly(ethylene oxide), Macromolecules 35 (9) (2002) 3681–3685.
[22] A. Harada, K. Kataoka, Formation of polyion complex micelles in an aqueous milieu from a pair of oppositely-charged block copolymers with poly(ethylene glycol) segments, Macromolecules 28 (15) (1995) 5294–5299.
[23] G. Majno, I. Joris, Apoptosis, oncosis, and necrosis. An overview of cell death, Am. J. Phathol. 146 (1) (1995) 3–15.
[24] K. Berg, P.K. Selbo, L. Prasmickaite, T.E. Tjelle, K. Sandvig, J. Moan, G. Gaudernack, O. Fodstad, S. Kjolsrud, H. Anholt, G.H. Rodal, S.K. Rodal, A. Hogset, Photochemical internalization: a novel technology for delivery of macromolecules into cytosol, Cancer Res. 59 (6) (1999) 1180–1183.
[25] A. Hogset, L. Prasmickaite, P.K. Selbo, M. Hellum, B.O. Engesaeter, A. Bonsted, K. Berg, Photochemical internalization in drug and gene delivery, Adv. Drug Deliv. Rev. 56 (1) (2004) 95–115.
[26] N. Nishiyama, Arnida, W.-D. Jang, K. Date, K. Miyata, K. Kataoka, Photochemical enhancement of transgene expression by polymeric micelles incorporating plasmid DNA and dendrimer-based photosensitizer, J. Drug Target. 14 (6) (2006) 413–424.
[27] N. Nishiyama, A. Iriyama, W.D. Jang, K. Miyata, K. Itaka, Y. Inoue, H. Takahashi, Y. Yanagi, Y. Tamaki, H. Koyama, K. Kataoka, Light-induced gene transfer from packaged DNA enveloped in a dendrimeric photosensitizer, Nature Mater. 4 (12) (2005) 934–941.
[28] C.S. Downes, M.J. Ord, A.M. Mullinger, A.R. Collinsm, R.T. Johnson, Novobiocin inhibition of DNA excision repair may occur through effects on mitochondrial structure and ATP metabolism, not on repair topoisomerases, Carcinogenesis 6 (9) (1985) 1343–1352.

Pharmaceutical Research, Vol. 26, No. 1, January 2009 (© 2008)
DOI: 10.1007/s11095-008-9712-2

Research Paper

A Photo-Activated Targeting Chemotherapy Using Glutathione Sensitive Camptothecin-Loaded Polymeric Micelles

Horacio Cabral,[2] Masataka Nakanishi,[1] Michiaki Kumagai,[2] Woo-Dong Jang,[4] Nobuhiro Nishiyama,[2,3] and Kazunori Kataoka[1,2,3,5]

Received June 21, 2008; accepted August 14, 2008; published online August 30, 2008

Purpose. A novel photo-activated targeted chemotherapy was developed by photochemical internalization (PCI) of glutathione-sensitive polymeric micelles incorporating camptothecin (CPT) prepared from thiolated CPT (CPT-DP) and thiolated poly(ethylene glycol)-*b*-poly(glutamic acid) (PEG-*b*-P(Glu-DP))
Methods. PEG-b-P(Glu-DP) and CPT-DP were synthesized and characterized by ^{1}H-NMR and gel permeation chromatography, and then mixed to prepare CPT-loaded polymeric micelles (CPT/m). The CPT release from the micelle was studied by reverse phase liquid chromatography. The PCI-activated cytotoxicity of CPT/m against HeLa cells was studied in combination with a non-toxic concentration of dendrimer phthalocyanine-loaded micelles (DPc/m) as the photosensitizer.
Results. The diameter of CPT/m was 96 nm and the drug loading was 20% (*w/w*). CPT was slowly released under the conditions reproducing the extracellular or endosomal environments. However, under the reductive conditions mimicking the cytosol, CPT was rapidly released achieving approximately 90% of the drug release after 24 h. The cytotoxicity of CPT/m was drastically increased on photoirradiation, whereas the CPT/m were not cytotoxic without PCI.
Conclusions. The CPT/m released the drug responding to reductive conditions. The PCI-induced endosomal escape exposed CPT/m to the cytosol triggering the drug release. Thus, CPT/m in combination with DPc/m will behave as smart nanocarriers activated only at photoirradiated tissues.

KEY WORDS: camptothecin; chemotherapy; environment sensitive-polymeric micelles; photochemical internalization.

INTRODUCTION

The site-specific drug delivery has become a key issue in cancer therapy, as the use of chemotherapeutic agents is often limited due to severe side effects, and the development of stimuli-responsive drug delivery systems that allow selective activation of the drugs at the target site will be crucial for successful therapies. In this way, the use of light for the activation of drug carriers is an attractive strategy because it is a safe energy source and it offers a high level of control in terms of wavelength, duration, intensity, and site of the photoirradiation, which can modulate the quantity of drug released, the timing of the release event and its location. The existing photoactivated drug delivery systems are mainly triggered by UV light, such as the systems based on the photoisomerization of azobenzene derivatives (1–5). Nevertheless, these systems are not suitable for biological applications because of the high absorbance of UV light by many biomolecules and the potential damage healthy tissues. Thus, it is necessary to develop realistic drug delivery systems activated by light with a longer wavelength in order to minimize photoinduced damage and to increase the depth of light penetration into tissues.

Recently, several macromolecules and other molecules that do not readily penetrate the plasma membrane have been used in combination with photochemical internalization (PCI) for the site-specific enhancement of their therapeutic efficacy by selective photochemical rupture of endocytic vesicles and consequent release of endocytosed macromolecules into the cytosol (6–13). The PCI concept is based on the

Electronic supplementary material The online version of this article (doi:10.1007/s11095-008-9712-2) contains supplementary material, which is available to authorized users.

[1] Department of Materials Engineering, Graduate School of Engineering, The University of Tokyo, 7-3-1 Hongo, Bunkyo-ku, Tokyo 113-8656, Japan.
[2] Center for Disease Biology and Integrative Medicine, Graduate School of Medicine, The University of Tokyo, 7-3-1 Hongo, Bunkyo-ku, Tokyo 113-0033, Japan.
[3] Center for NanoBio Integration, The University of Tokyo, 7-3-1 Hongo, Bunkyo-ku, Tokyo 113-8656, Japan.
[4] Department of Chemistry, College of Science, Yonsei University, Seoul, South Korea.
[5] To whom correspondence should be addressed. (e-mail: kataoka@bmw.t.u-tokyo.ac.jp)

ABBREVIATIONS: CPT, camptothecin; CPT-DP, thiolated CPT; PEG-*b*-P(Glu-DP), thiolated poly(ethylene glycol)-*b*-poly(glutamic acid); CPT/m, CPT-loaded polymeric micelles; DLS, dynamic light scattering; DPc/m, dendrimer phthalocyanine-loaded micelles; PCI, photochemical internalization; PDT, photodynamic therapy; PS, photosensitizer; SPTDP, disulfide amine linker; RPLC, reverse phase liquid chromatography.

use of photosensitizers, which induce the formation of reactive oxygen upon exposure to light of appropriate wavelengths (14). These photochemical reactions are the basis for photodynamic therapy (PDT), a treatment modality where light exposure leads to photosensitizer-induced killing of cancer cells used in various types of cancer (15,16). The PCI allows macromolecules located in the vesicles to reach the cytosol and to exert their biological activity instead of being degraded by lysosomal hydrolases. Furthermore, this PCI-based relocalization and activation of the macromolecules has the advantage of minimal side effects because the effect is localized to the irradiated area. The PCI employs light with clinically relevant wavelengths even in the near IR region, allowing a therapeutic effect in deeper lesions of the target tissues and a negligible damage to healthy tissue. In addition, after PCI, the macromolecules are exposed to the extremely reductive environment of the cytosol. Since the concentration of glutathione at the cytosol is 100–1,000 times higher than that in blood (17), it can be used as an efficient stimulus for the specific drug carrier activation. Consequently, the combination of PCI and drug carriers responsive to reductive environment will present the spatial and temporal triggering of drug action by photoirradiation.

The PCI-induced chemotherapy should be performed utilizing drug carriers that selectively accumulate in tumor tissues and enter cells *via* endocytosis. In this way, the polymeric micelles have shown reduced non-specific accumulation in normal tissues and preferential accumulation in solid tumors by the enhanced permeability and retention effect (18–22). Previously, we have reported polymeric micelles for the delivery of chemotherapeutics and photosensitizing agents with enhanced activity both *in vitro* and *in vivo* (11–13,18,20,23,24). Moreover, we have utilized dendrimer phthalocyanine (DPc)-loaded polymeric micelles (DPc/m), as photosensitizers, to increase the transfection efficiency of polyion complex micelles incorporating plasmid DNA by PCI (11–13). Thus, in the present study, we will utilize DPc/m to induce PCI for the specific activation of glutathione-sensitive camptothecin (CPT)-loaded polymeric micelles (CPT/m). Since both the CPT/m and the DPc/m are expected to exhibit prolonged blood circulation, selectively accumulate in tumor tissues and be taken up by cancer cells *via* endocytosis as previously reported for similar systems (18–21; Fig. 1), the combination will behave as a photoactivated drug delivery system for *in vivo* application.

CPT and its derivatives are very potent antitumor agents (25), though their full clinical potentials have yet to be realized because of the lack of water-solubility, the instability of the pharmacologically active lactone ring and the fast non-specific distribution to the whole body (25,26). Thus, the development of adequate carriers for the delivery of CPT is imperative. Herein, the CPT/m were prepared by conjugating a thiolated-camptothecin derivative (CPT-DP) to thiolated poly(ethylene glycol)-poly(glutamic acid) [PEG-*b*-P(Glu-DP)] block copolymer *via* a disulfide bond given that this bond is stable in blood and specifically cleaved in a reductive environment (17). Accordingly, the *in vitro* release profiles were studied under different conditions. Moreover, in order to prove the concept of a photoactivated drug delivery system, we tested the ability of CPT/m combined with a non-toxic concentration of DPc/m to specifically eradicate cancer cells *in vitro* after photoirradiation.

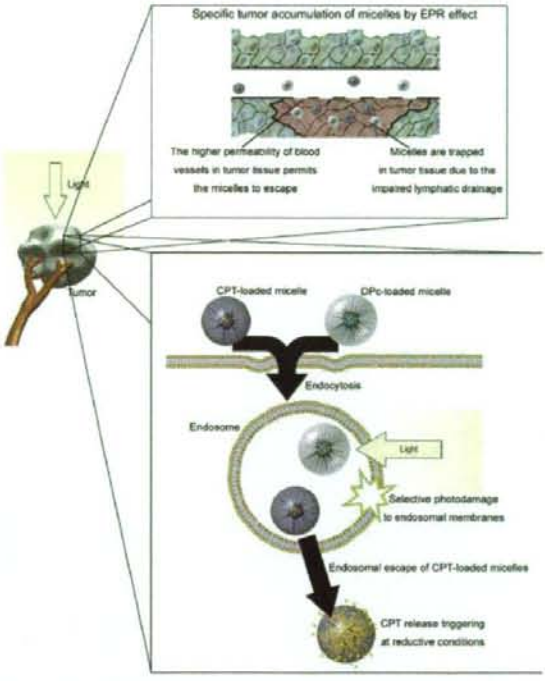

Fig. 1. Photochemical internalization-activated targeting chemotherapy. The polymeric micelles encapsulating camptothecin (*CPT*) and dendrimer phthalocyanine (*DPc*) accumulate in tumor tissue by the enhanced permeability and retention effect. The tumor is irradiated at the relevant wavelength. Both micelles are considered to be taken up by the cell through the endocytic pathway. The localization of the *DPc-loaded micelles* in the endosome allows the selective photodamage of the endosomal membrane upon photoirradiation, thereby inducing the endosomal escape of *CPT-loaded micelles* and the selective release of CPT under reductive conditions.

MATERIALS AND METHODS

Materials

γ-Benzyl L-glutamate and *N*-z-L-lysine were bought from Sigma Chemical Co., Inc. (St. Louis, MO, USA). Bis(trichloromethyl)carbonate (triphosgene) was purchased from Tokyo Kasei Kogyo Co., Inc. (Tokyo, Japan). Dichloromethane, 4-dimethylaminopyridine (DMAP), dicyclohexylcarbodiimide (DCC), camptothecin, *N,N*-Dimethylformamide (DMF), dimethyl sulfoxide (DMSO), dithiothreitol (DTT) and 3-(4,5-dimethylthiazol-2-yl)-2,5-diphenyltetrazolium bromide (MTT) were obtained from Wako Pure Chemical Co., Inc. (Osaka, Japan). Methoxycarbonylsulfenyl chloride, 2-mercaptopyridine and 3-mercaptopropionic acid were purchased from Aldrich Chemical Co., Inc. (Milwaukee, WI, USA). α-Methoxy-ω-aminopoly(ethylene glycol) (CH_3O-PEG-NH_2; Mw=5,000 and 12,000) was purchased from Nippon Oil and Fats Co., Inc. (Tokyo, Japan). All solvents for the polymer syntheses were distilled just before use.

Cell Lines

Human cervical carcinoma HeLa cells were supplied from Japanese Collection of Research Bioresources Cell Bank (Osaka, Japan). HeLa cells were maintained in Dulbecco's Modified Eagle Medium (DMEM; Sigma Chemical Co., Inc.) containing 10% fetal bovine serum in a humidified atmosphere containing 5% CO_2 at 37°C.

Synthesis of Thiolated Camptothecin (CPT-DP)

A CPT derivative bearing the pyridyl disulfide group was synthesized as shown in Fig. 2. Briefly, a solution of methoxycarbonylsulfenyl chloride (1.25 g, 3.8 mmol) in methylene chloride (26 ml) was treated with 3-mercaptopropionic acid (1.05 g, 3.8 mmol) in methylene chloride (13 ml) for 2 h. After solvent was evaporated, the residue was redissolved in methylene chloride (26 ml) and treated dropwise with a solution of 2-mercaptopyridine (1.1 g, 3.8 ml) in 13 ml of the same solvent. After stirring overnight, the solvent was evaporated to yield an oily residue of 3-(2-pyrinyldithio)propionic acid. Then, 0.5 mmol of 3-(2-pyrinyldithio)propionic acid was mixed with 0.5 mmol CPT, 0.55 mmol DMAP and 0.55 mmol EDC in 5 ml methylene chloride. After 24 h stirring at room temperature, the mixture was diluted with 150 ml methylene chloride and washed with 0.01 N HCl (30 ml, one time) and water (30 ml, six times). The organic layer was evaporated to obtain a pale orange solid. The product was purified by silica gel chromatography using methylene chloride-methanol (97:3 *v/v*) as an eluent to yield an orange solid of CPT-DP. The proper modification of CPT was analyzed by ^{1}H-NMR in DMSO at 25°C

Synthesis of Thiolated Poly(ethylene glycol)-Poly(glutamic acid) [PEG-*b*-P(Glu-DP)] Block Copolymer

Preparation of Disulfide Amine Linker

Thiopyridyl disulfide was dissolved in 20 ml of methanol and 0.8 ml of acetic acid. Into this solution was added dropwise over a period of 0.5 h 2-aminoethylthiol hydrochloride in 10 ml methanol. The mixture was stirred for 48 h and then evaporated to yield yellow oil, followed by washing with 50 ml diethyl ether and dissolution in 10 ml of methanol. The product was precipitated by addition of 200 ml of diethyl ether, chilled for 12 h at −20°C and collected by vacuum filtration (yield: 77%).

Synthesis of Poly(ethylene glycol)-Poly(glutamic acid) [PEG-b-P(Glu)] Block Copolymer

PEG-P(Glu) block copolymer was synthesized according to the previously described synthetic method (27). Briefly, the *N*-carboxy anhydride of γ-benzyl L-glutamate (BLG-NCA) was synthesized by the Fuchs–Farthing method using triphosgene. Then, BLG-NCA was polymerized in DMF, initiated by the primary amino group of CH_3O-PEG-NH_2, to obtain PEG-poly (γ-benzyl L-glutamate) (PEG-b-PBLG) block copolymer. The molecular weight distribution of PEG-b-PBLG was determined by gel permeation chromatography [column: TSK-gel G3000HHR, G4000HHR (Tosoh Co., Inc., Yamaguchi, Japan); eluent: DMF containing 10 mM LiCl; flow rate—0.8 ml/min; detector: refractive index; temperature: 25°C]. The polymerization degree of PBLG was verified by comparing the proton ratios of the methylene units in PEG ($-OCH_2CH_2-$: δ= 3.7 ppm) and the phenyl groups of PBLG ($-CH_2C_6H_5$: δ= 7.3 ppm) in ^{1}H-NMR spectrum (solvent: DMSO-d_6; temperature: 80°C), and it was determined to be 81. The deprotection of the benzyl group of PEG-b-PBLG was carried out by mixing with 0.5 N NaOH at room temperature to obtain PEG-P(Glu).

Synthesis of Thiolated Poly(ethylene glycol)-b-Poly(glutamic acid) [PEG-b-P(Glu-DP)] Block Copolymer

The P(Glu) backbone of PEG-b-P(Glu) was thiolated by the procedure illustrated in the Fig. 3. Briefly, PEG-b-P (Glu) was dissolved in DMSO, followed by addition of NHS and water soluble DCC. The solution was stirred for 2 h, and

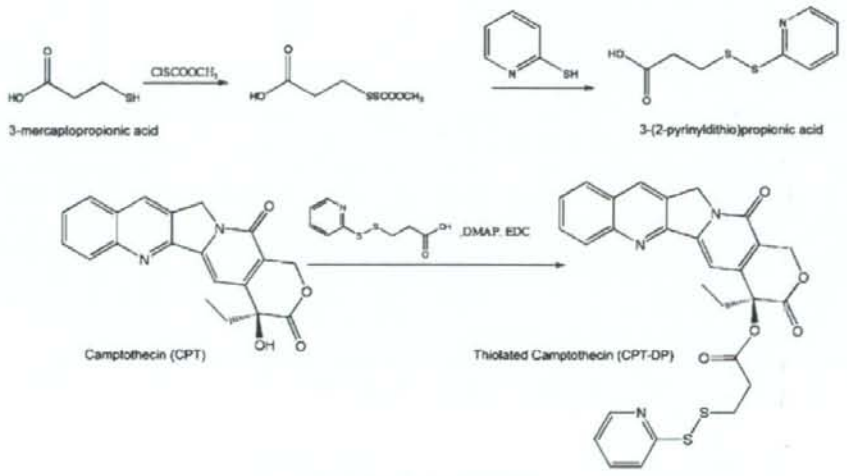

Fig. 2. Synthesis of CPT-DP.

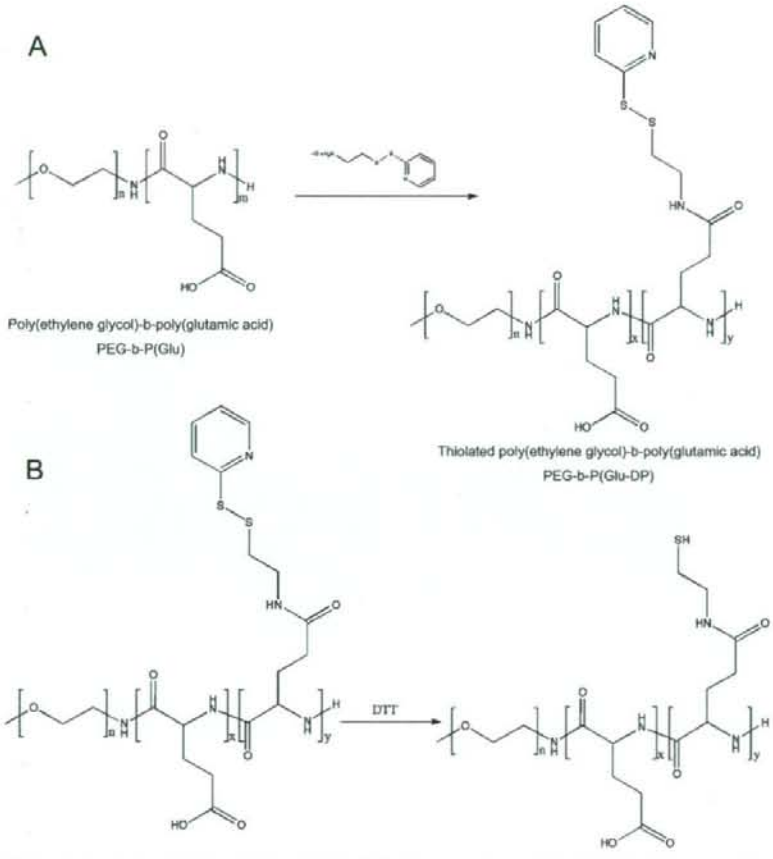

Fig. 3. **A** Synthesis of thiolated (PEG-*b*-P(Glu-DP) **B** Deprotection of PEG-*b*-P(Glu-DP) using DTT.

then SPTDP was added. The solution was stirred for another 20 h. Then, the mixture was dialyzed against water and finally freeze-dried. The characterization of the polymer was performed by ^{1}H-NMR (solvent: DMSO-d6; temperature: 80°C).

Preparation of Camptothecin-loaded Micelle (CPT/m)

CPT/m were prepared as follows: PEG-*b*-P(Glu-DP) (60 mg) was mixed with DTT (3-fold excess) in DMSO in order to deprotect the sulfide group at the *p*(Glu) backbone. Twenty-four hours later, the solution was dialyzed against DMSO. After dialysis, CPT-DP, (40 mg) was added and the solution was shaken at 37°C in dark for 72 h. Then, the unreacted CPT-DP was removed by dialysis against DMSO. The resulting drug-polymer conjugate was dialyzed against water in order to form polymeric micelles. Finally, the micelle solution was purified by ultrafiltration (MWCO—50,000) and the size distribution of the micelle was measured by dynamic light scattering (DLS) using a Zetasizer Nano ZS90 (Malvern Instruments Ltd., Worcestershire, United Kingdom). The CPT concentration of micelle solution was determined by reverse phase liquid chromatography (RPLC) [column: μ-Bondasphere (Waters, Japan); eluent: acetonitrile/1% acetic acid; detector: fluorescence (emission—370 nm; detection—440 nm); temperature: 40°C] after micelle dissociation with 10 mM DTT and mixing in 1 N HCl.

Synthesis of Dendrimer Phthalocyanine

The synthesis of the ionic DPc was performed according to the method reported by Ng's group (28). The second generation of dendritic phenol was reacted with 4-nitrophtalonitrile by an alkali-mediated coupling reaction to obtain the corresponding dendritic phthalonitrile, which was treated with Zn $(OAc)_2$ and 1,8-diazabicyclo[5.4.0]undec-7-ene (DBU) in *n*-pentanol to give DPc. The obtained DPc was 4,904 dalton and the adsorption spectra in an aqueous solution revealed that DPc exhibits a B band absorption at 350 nm and a strong Q band absorption at 685 nm, indicating a monomeric dispersion (24).

Synthesis of Poly(ethylene glycol)–*b*-poly(*l*-Lysine) [PEG-*b*-PLL]

PEG-*b*-PLL block copolymer was synthesized as previously reported (29). Briefly, the *N*-carboxy anhydride of *N*-Z-Lysine was polymerized from the ω-NH_2 group of CH_3O-PEG-NH_2 in DMF under Ar to obtain PEG-*b*-PLL(Z), followed by the

deprotection of the Z group. The polymerization degree of the PLL segments was determined to be 49 by ^{1}H-NMR.

Preparation of Dendrimer Phthalocyanine-loaded Micelle

The DPc/m was prepared as previously described (24). Briefly, DPc was dissolved in 10 mM Na_2HPO_4 (1 ml) and added to PEG-*b*-PLL in a 10 mM NaH_2PO_4 (0.457 ml) to give a solution containing DPc/m in 10 mM phosphate buffered solution (pH 7.4). The size distribution of DPc/m was determined by DLS.

CTP Release from CPT/m under Different Conditions

The release of CPT from the micelle under different conditions was evaluated by the dialysis method. Briefly, a micellar solution of known CPT concentration was placed inside a dialysis bag and dialyzed against 10 mM PBS plus 150 mM NaCl (pH 5 and 7.4) or 10 mM PBS plus 3 mM DTT at 37°C. The solution outside the dialysis bag was sampled at defined time periods to determine the amount of free CPT released from the micelle. Then, 0.1 ml of the sample was diluted in 0.4 ml of 1 N HCl, and the concentration was measured by RPLC using the conditions previously described.

In Vitro Photocytotoxicity of DPc/m

In order to determine the non-toxic concentration of DPc/m that will be used for the PCI of CPT/m, the growth-inhibitory activity of the DPc/m was evaluated by MTT assay. HeLa cells were cultured in DMEM containing 10% FBS in 96-well multiplate. After 24 h incubation, cells were incubated with the drugs for 24 h, followed by photoirradiation for 10 min using a 300 W halogen lamp (fluence rate: 3.0 mW cm^{-2}) equipped with a band-pass filter (400–700 nm). Then, the cells were post-incubated for 24 and 48 h. The cell viability was measured by MTT assay.

PCI-enhanced *In Vitro* Cytotoxicity of Camptothecin-loaded Micelle

The growth-inhibitory activity of the free CPT, free CPT-DP and CPT/m with and without a non-toxic concentration of DPc/m was evaluated by MTT assay. HeLa cells were cultured in DMEM containing 10% FBS in 96-well multiplate. After 24 h incubation, the cells were exposed to each CPT formulation in the combination with DPc/m. Twenty-four hours after drug exposure, the cells were photoirradiated 10 min. Then, the cells were post-incubated for 24 and 48 h. Finally, MTT solution was added and, 3 h later, 20% SDS solution was added. Cell viability was measured by the formed formazan absorbance at 570 nm.

RESULTS

CPT-loaded Micelle

The proper incorporation of the linkers to CPT and PEG-*b*-P(Glu) was confirmed by ^{1}H-NMR. After column purification, the spectra of CPT-DP presented the proton peaks corresponding to the CPT plus the alkyl-disulfide-pyridine linker (Fig. 4). From the proton ratio between the methylene group *j* of CPT (Fig. 4A) and the methylene protons, *1* or *2*, of the conjugated linker, the degree of modification of CPT was determined to be 100% by ^{1}H-NMR (Fig. 4B). Moreover, the RPLC results showed a single peak suggesting high purity of the product (Fig. 4C). For the PEG-*b*-P(Glu-DP), the degree

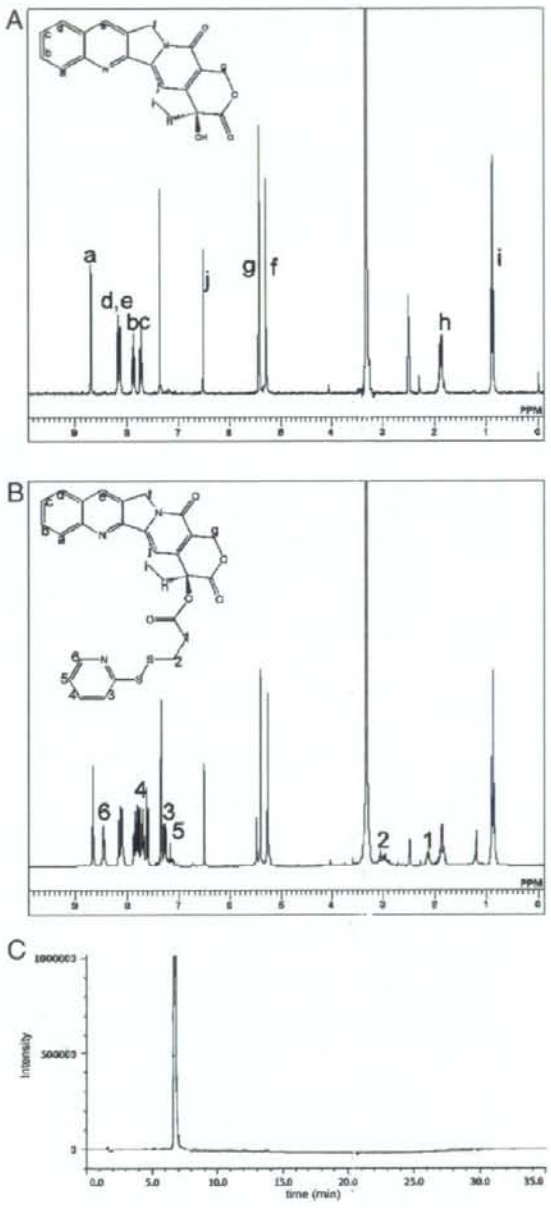

Fig. 4. Characterization of the thiolated camptothecin derivative. **A** ^{1}H-NMR spectra of CPT; **B** ^{1}H-NMR spectra of thiolated camptothecin (CPT-DP); **C** RPLC chromatogram of CPT-DP.

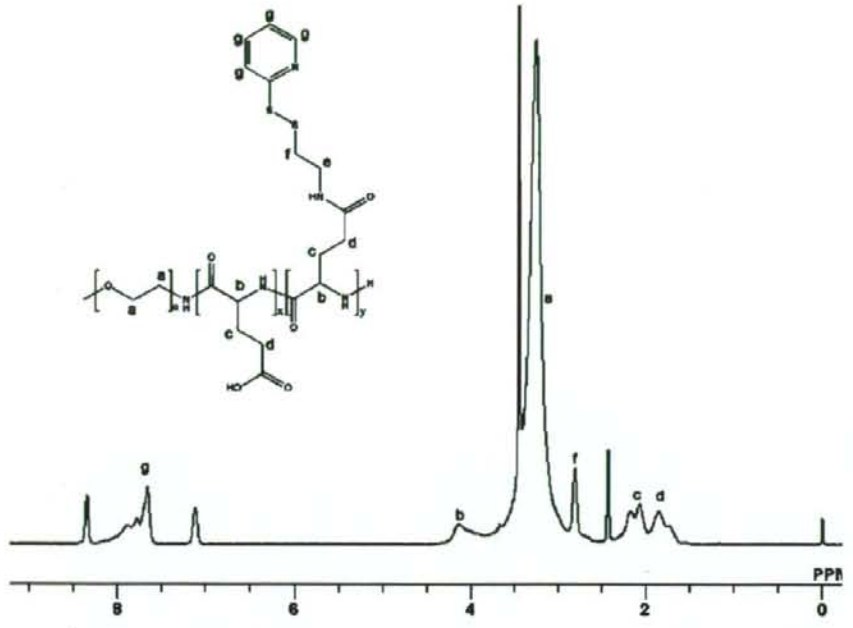

Fig. 5. ^{1}H-NMR spectra of thiolated poly(ethylene glycol)-poly(glutamic acid) block copolymer (PEG-*b*-P (Glu-DP)).

of thiolation was determined to be 44 [54% of the P(Glu) units] by comparing the proton ratios of the methylene units in PEG (–OCH_2CH_2–: δ=3.7 ppm) and the pyridine groups of P (Glu-DP) (–CH_5H_4N: δ=7.5 ppm; Fig. 5).

The driving force for micelle assembly is the hydrophobic interaction between P(Glu-DP) backbones of the block copolymers after the conjugation of CPT-DP. After purification of the micelles by ultrafiltration, the size distribution of CPT/m was determined to be 96.3 nm with a considerable low cumulant polydispersity (μ_2/Γ^2=0.048) by DLS. In addition, the CPT/m formulation offers the possibility to be lyophilized for long-term storage. After redissolving the freeze-dried CPT/m in water, the DLS results showed a z-average diameter of 100 nm and a polydispersity of 0.1. Note that the size of a colloidal drug carrier is a determinant feature of its fate in blood circulation and its biodistribution. The sub-100 nm size as well as the hydrophilic PEG palisade surrounding the core are important features of the CPT/m to avoid their uptake by the reticuloendothelial system.

The drug loading was estimated after micelle dissociation with 10 mM DTT by RPLC. The incorporated amount was determined to be 0.25 CPT molecules per thiol group at the p (Glu) backbone ([CPT-S]/[SH]), indicating 20% of CPT to PEG-*b*-P(Glu-DP) (*w*/*w*). This corresponds to approximately 35% of the initial CPT-DP feeding. Worth mentioning is that the thiol moieties in the P(Glu-DP) backbone that did not react with CPT may form disulfide bonds to crosslink the micellar core. We previously reported that similar micellar systems show complete disulfide bond formation by spontaneous oxidation of the thiol groups in the solution (30–32). Such disulfide crosslinks may stabilize the micelle structure in addition to the hydrophobic interaction.

Release Rate from CPT/m under Different Conditions

Drug-loaded micelles should be designed to release their contents after reaching the targeted tissue since the premature drug release can lead to toxic effects. Hence, the CPT release rate was studied under different conditions simulating different biological environments (Fig. 6). At settings that reproduce the extracellular environments, i.e. 10 mM phosphate buffer pH 7.4 plus 150 mM NaCl, the CPT release from the micelle was extremely low. After 96 h, the release was determined to be almost 30% of the incorporated CPT (Fig. 6). At endosomal pH, i.e. pH 5.5, the percentage of drug released from the micelle core was also found to be very low with approximately 1% of the drug released after 96 h (Fig. 6). Nevertheless, in a reductive environment simulating the cytosolic conditions, 10 mM PBS plus 3 mM DTT, a burst release of CPT was observed throughout the first 10 h. During this period, almost 80% of the incorporated drug was released. Then, the drug release reached a plateau achieving more than 90% of the drug released in 96 h (Fig. 6). This fast and preferential drug release under cytosolic conditions can be exploited to deliver CPT only in tissues where the micelles can escape from the endosomes aided by PCI.

In Vitro Photocytotoxicity of DPc/m

Hela cells were incubated with different concentrations of DPc/m for 24 h. Then, HeLa cells were photoirradiated at the fluence rate of 3.0 mW/cm^2 for 10 min (fluence—1.8 J/cm^2) and then post-incubated for 24 and 48 h. The results presented a DPc concentration-dependent decrease in cell viability (Fig. 7A and B). The photo-induced cell death is observed at the region of high DPc concentrations, and it

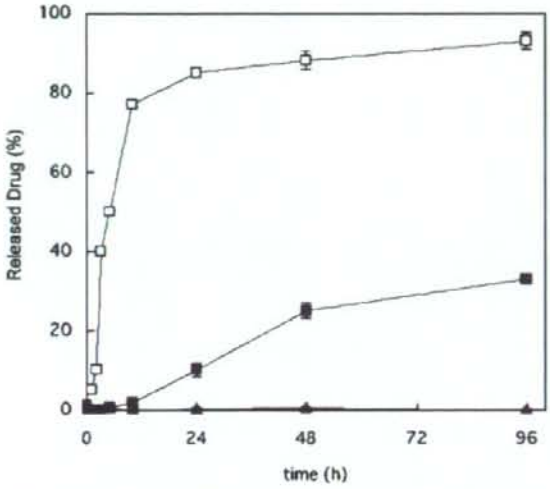

Fig. 6. Release rate of CPT-DP from the micelles (CPT/m) at 10 mM phosphate buffer plus 150 mM NaCl at pH 5.5 (*filled triangle*); pH 7.4 (*filled square*); and 3 mM DTT (*unfilled square*). Determined by RPLC (acetonitrile:1% acetic; fluorescence emission: 370 nm; fluorescence detection—440 nm). Data are shown as mean ± SD (n=3).

might be attributable to the vast photochemical reactions. At low DPc concentrations, the production of reactive oxygen species may be low and mainly confined to the endosomal compartments, maintaining the cell viability. Thus, in order to minimize the photocytoxicity from the DPc/m in the following PCI-mediated enhancement of CPT/m, a non-toxic concentration of DPc/m was determined. The highest non-toxic concentration of dendrimer-micelle was observed at 1×10^{-3} mg/ml. Therefore, the DPc/m concentration was fixed at 1×10^{-4} mg/ml for the following experiments.

PCI-Enhanced *In Vitro* Cytotoxicity of CPT/m

The cytotoxicity of free CPT, free CPT-DP and CPT/m in combination with the non-toxic concentration of DPc/m with and without photoirradiation against HeLa cells is shown in Figs. 8 and 9, and IC50 values are summarized in Table I. As shown in Fig. 8 and Table I, free CPT-DP showed slightly higher cytotoxicity than free CPT, which may be due to facilitated cellular uptake of CPT-DP with a hydrophobic pyridyl disulfide group. In the presence of photoirradiation, the combination of free CPT or CPT-DP and DPc/m showed less than 2-fold enhancement of the cytotoxicity without photoirradiation. Because free CPT or CPT-DP enter cells by passive diffusion and show potent cytotoxicity without photoirradiation, there may be a synergistic effect between cytotoxic compounds (i.e., fee CPT and CPT-DP) and photodynamic effect by DPc/m. This effect is assumed to be the combination effect of chemotherapy and PDT rather than PCI, since PCI is aimed to deliver cell membrane-impermeable drugs and macromolecular compounds from the endo-/lysosomes to the cytosol through the photochemical disruption of endo-/lysosomal membranes, thus achieving the light-selective drug action (9). On the other hand, the combination of CPT/m and DPc/m without photoirradiation was not toxic after 24 h post-incubation, probably due to the localization of the micelles in the endosome and the restricted drug release of CPT/m (Fig. 9A). However, when the cells were photoirradiated, the PCI effect exposed the CPT/m to the reductive conditions of the cytosol by endomal escape. Hence, the *in vitro* cytotoxicity of CPT/m was considerably increased (Fig. 9A), suggesting that the antitumor activity of CPT/m can be significantly enhanced by photoirradiation. At 48 h, the combination of CPT/m and DPc/m without photoirradiation slightly decreased the cell viability at high CPT/m concentrations (Fig. 9B). Nevertheless, the PCI using DPc/m significantly enhanced the antitumor activity of CPT/m at 48 h (Fig. 9B). Thus, as shown in Table I, the combination of CPT/m and DPc/m achieved remarkable (6.5-fold or much more) enhancement of the cytotoxiciy by photoirradiation.

DISCUSSION

Berg and Høgset *et al.* were the first to combine PCI and chemotherapy to deliberately increase the internalization of the anticancer drug bleomycin (33). The PCI-mediated relocalization of bleomycin into the cytosol considerably enhanced its *in vitro* and *in vivo* efficacy because bleomycin is practically non-permeant to the plasma membrane and enters the cells by endocytosis whereby it may be degraded in the lysosomes. Nevertheless, bleomycin is in contrast to traditional anticancer agents, such as CPT, that will easily pass the cell membrane and will generally be taken up by non-target cells generating severe side effects. Therefore, the PCI site-specific targeting of traditional anticancer drugs should be performed using drug carriers that enter the cells *via* endocytosis and release their contents only after PCI. In this way, the CPT/m presented a strong *in vitro* cytotoxicity after endosomal escape by PCI. The carrier activation is correlated with the fast CPT release from the micelle core under reductive conditions. Moreover, the modification of the outer hydrophilic shell of CPT/m with cancer-specific ligands can increase the specific uptake in tumor cells and the efficiency will be considerably enhanced.

The CPT/m were also designed to release their contents after reaching the targeted tissue. Like this, the drug leakage from CPT/m during blood circulation will be minimized since the experiments of drug release rate demonstrated that the disulfide linker used to conjugate CPT to the block copolymer backbone is selectively cleaved under reductive conditions. This will reduce the toxic effects that arise from non-specific accumulation of free drug. Moreover, the delivery of the active lactone form of CPT is also crucial for exerting the antitumor activity. In this way, it has been determined that modifying CPT at the 20 position as an ester stabilizes the active lactone ring under physiological conditions (34). Accordingly, the CPT instability under physiological conditions may also be reduced for the CPT-DP derivative. In addition, previous studies revealed that the lactone ring of CPT was protected upon incorporation of the drug into the lipid bilayer of liposomes (35,36), microspheres (37,38), nanobiohybrids (39), and polymeric micelles (40,41). Thus, the hydrophobic core of CPT/m probably functions as an auspicious CPT reservoir by inhibiting drug inactivation. In addition, after the PCI, the CPT/m will reach the interior of cancer cells, release the CPT in the lactone form avoiding extracellular inactivation and, in this way, maximize the efficiency of CPT.

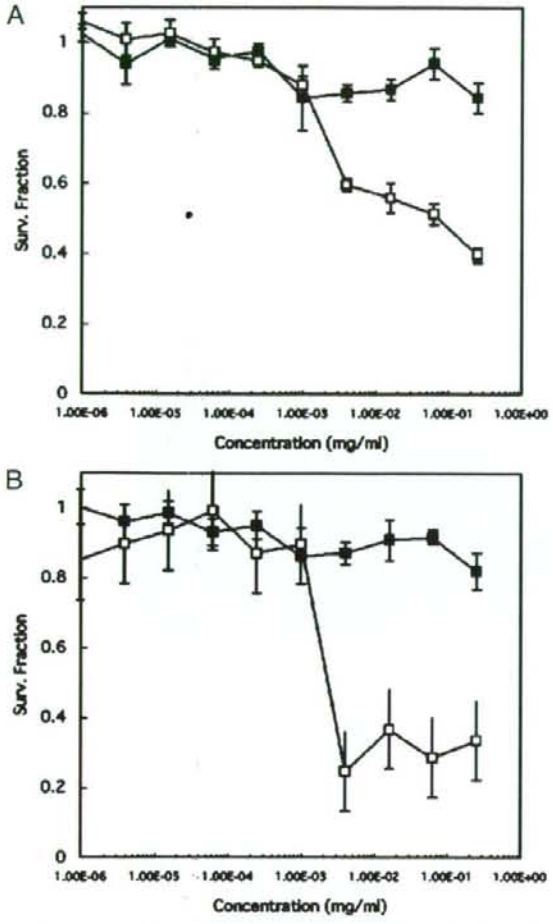

Fig. 7. Cell viability of dendrimer phthalocyanine-loaded polymeric micelles (DPc/m) without irradiation (*filled square*) and with 10 min irradiation at a fluence of 1.8 J/cm2 (*unfilled square*). **A** 24 h incubation after photoirradiation; **B** 48 h incubation after photoirradiation. Data are shown as mean ± SD (n=4).

In this study, we successfully achieved the light-induced activation of chemotherapeutic agents by the PCI using the combination of CPT/m and DPc/m under the condition at which the photosensitizer (PS) alone showed no photocytotoxicity. Although there are several previous reports regarding the photo-activated chemotherapy using the combination of chemotherapeutic agents and PSs, in those studies the light-induced enhancement of the cytotoxicity of chemotherapeutic agents was observed only when the PS alone showed significant photocytotoxicity (42,43). The highly light-selective activation of chemotherapeutic agents by our system may be attributed to (1) the aforementioned CPT release selectively after the endosomal escape of CPT/m by the PCI and (2) highly selective photodamage to the endo-/lysosomal compartments by DPc/m. It is reported that low-molecular weight PSs such as sulfonated phthalocyanine ($AlPcS_{2a}$), which were used in other studies, show significant photocytotoxicity accompanied by the PCI (8,9), probably because they are assumed to accumulate not only in the endo-/lysosomes but also in other organelles susceptible to the photodamage such as the plasma membranes and mitochondria. In contrast, DPc/m is assumed to accumulate selectively in the endo-/lysosomes, thereby achieving the PCI without compromising the cytotoxicity. Regarding the intracellular behaviors of DPc/m upon photoirradiation, we previously reported that DPc/m showed 100-fold higher *in vitro* photocytotoxicity against HeLa cells than free DPc, which cannot be explained by four times higher cellular uptake of DPc/m compared with free DPc (24). Therefore, it appears that DPc/m in a micellar form should play a pivotal role in the intracellular photochemical reactions rather than released free DPc. Indeed, we confirmed that the physicochemical

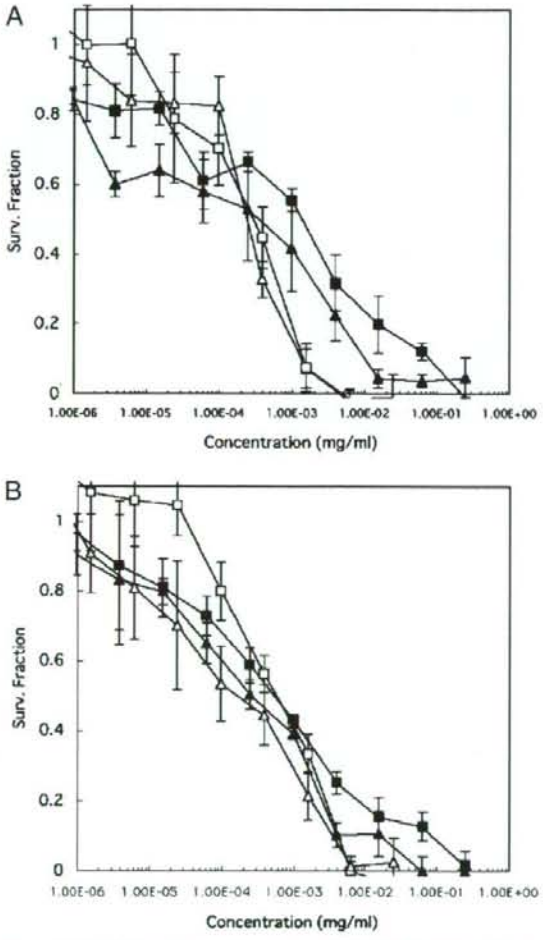

Fig. 8. Cell viability after treatment with CPT and CPT-DP combined with a non-toxic concentration of DPc/m with and without 10 min irradiation at a fluence of 1.8 J/cm^2. **A** 24 h incubation after photoirradiation; **B** 48 h incubation after photoirradiation. Non-photoirradiated CPT plus DPc/m, *filled square*; non-photoirradiated CPT-DP plus DPc/m, *filled triangle*; photoirradiated CPT plus DPc/m, *unfilled square*; photoirradiated CPT-DP plus DPc/m, *unfilled triangle*. Data are shown as mean ± SD (n=4).

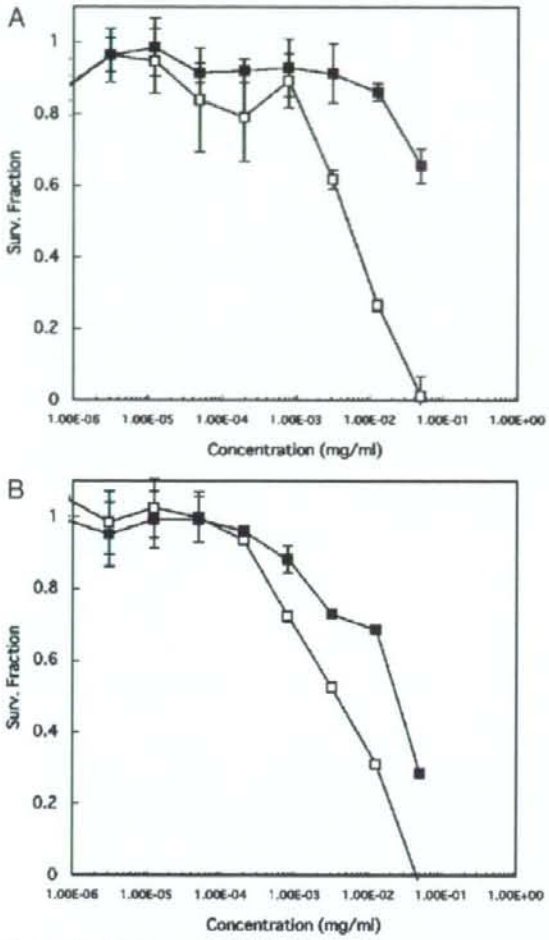

Fig. 9. Cell viability for CPT/m combined with a non-toxic concentration of DPc/m with and without 10 min irradiation at a fluence of 1.8 J/cm^2. **A** 24 h incubation after photoirradiation; **B** 48 h incubation after photoirradiation. Non-photoirradiated CPT-DP plus DPc/m, *filled square*; photoirradiated CPT/m plus DPc/m, *unfilled square*. Data are shown as mean ± SD (n=4).

properties (scattering light intensity, cumulant diameter and polydispersity index) of DPc/m were not changed during the photoirradation under the tested conditions in this study (Supporting Information). The detailed intracellular behaviors of DPc/m are now under investigation, and the results will be reported elsewhere in the near future.

Recent developments in fiber optics and laser technology allow illuminating many sites inside the human body, e.g. gastrointestinal tract, urogenital organs, lungs, brain and pancreas. However, as for PDT, one important *in vivo* restriction is the limited penetration of light into the tissue. In tissues, the light penetration decays approximately exponentially (e^{-1}) for every 2–3 mm, with a theoretical maximum for PDT effects of about 1 cm if a photosensitizer that absorbs in the far-red region of the light spectrum is used (9). For PCI, the penetration depth would be substantially larger, since very good PCI effects can be achieved with very feeble light doses. Accordingly, the penetration depths of light for effective PCI could be expected at approximately 2 cm (9). In addition, in the PCI-mediated chemotherapy, chemotherapeutic agents released from the nanocarriers after photoirradiation can diffuse through the tumor tissue, allowing the treatment of thicker and hypoxic tumors, which are known to be intractable by PDT alone due to the limited light penetration and low oxygen concentration, respectively. Another benefit of PDT and chemotherapy combination is that PDT has shown to overcome multidrug resistance in many *in vivo* tumor models (43). Recent *in vitro* results indicated that PCI has the ability to circumvent the multidrug resistance in adriamycin-resistant breast cancer MCF-7 cells by release of the adriamycin localized at end-/lysosomes after PCI (42, 44, 45).

CONCLUSION

We have designed a novel PCI-activated drug carrier for the delivery of CPT using the glutathione-sensitive polymeric micelle. The micelle showed very low release of free drug under physiological conditions. However, in the presence of a reductive agent (DTT), the drug release increased rapidly. The effect of PCI strikingly enhances the *in vitro* cytotoxicity of CPT/m by augmenting the micelle access to the cytosol. The PCI employing the combinational micelle formulations of DPc/m and CPT/m could allow the long-sought ability to deliver chemotherapeutics where, when, and in the required doses, thus maximizing their effect and reducing side effects and damage to healthy tissues. The present results not only

Table I. *In Vitro* Cytotoxicity of Free Camptothecin, Thiolated Camptothecin, CPT-Loaded Micelles Plus 1×10^{-4} mg/ml of Dendrimer Phthalocyanine-loaded Micelles Against HeLa Cells

Irradiation (min)	Post-incubation (h)	IC50 (μM)[a]		
		CPT + DPc/m	CPT-DP + DPc/m	CPT/m + DPc/m
0	24	2	1	N.D.
0	48	1.5	0.4	65
10[b]	24	1	0.7	20
10	48	1.5	0.2	10

CPT Camptothecin, *CPT-DP* thiolated camptothecin, *CPT/m* CPT-loaded micelles, *DPc/m* dendrimer phthalocyanine-loaded micelles
[a] IC50 value obtained by 3-(4,5-dimethylthiazol-2yl)-2,5-diphenyltetrazolium bromide assay
[b] Cells were photoirradiated at a fluence of 1.8 J/cm^2